Arterial hypertension.

Consume carbon monoxide?

George Shuang

Supervisor: Dr Martin Fronius

A thesis submitted in partial fulfilment of the requirements for the degree of Bachelor of Biomedical Sciences with Honours at the University of Otago, Dunedin, New Zealand.

October 2019

Abstract

Epithelial sodium channels (ENaC) are generally responsible for the passive movement of sodium ions through the apical cell membrane of salt absorbing epithelia. Canonical ENaC is composed of three homologous subunits, most commonly being a combination of alpha, beta, and gamma subunits (αβɣ-ENaC). However, in humans, ENaC has also been found to exist as a combination of delta, beta, and gamma subunits (δβɣ-ENaC).

ENaC subunits were also detected in the endothelium of arteries where they are exposed to shear stress from the blood flow. αβɣ-ENaC is known to be activated by shear stress and inhibit vascular relaxation potentially exacerbating the effects of hypertension. A potential new treatment option for hypertension is targeting arterial ENaC through carbon monoxide (CO). CO has been tested as an emerging potential treatment for cardiovascular disease and hypertension. Studies have shown conflicting effects of CO on αβɣ-ENaC activity. Currently the effect of CO on δβɣ-ENaC have been characterized, and how the effect of shear stress compared between αβγ-ENaC and δβγ-ENaC.

Therefore, I aimed to use Two Electrode Voltage Clamping (TEVC) and Xenopus laevis oocytes expressing αβɣ-ENaC or δβɣ-ENaC, to examine how both types of ENaCs respond to shear stress and CO. Our data shows δβɣ-ENaC responds to shear stress in a dose dependent manner that is less sensitive compared to the response seen in αβɣ-ENaC. This suggests δβɣ-ENaC may potentially play a role in hypertension, but further

experimentation is needed to confirm if it influences vascular relaxation like αβɣ-ENaC. Furthermore, no significant response was seen by both ENaCs towards carbon monoxide, but a strong biphasic trend was noted in δβɣ-ENaC that was not seen in αβɣ-ENaC. This suggests that carbon monoxide has potential in modulating αβɣ-ENaC activity that is based on concentration. Further experimentation to confirm this trend may place carbon monoxide as a potential therapeutic in the treatment of hypertension as well as explaining the conflicting results seen in literature as of currently.

Acknowledgements

First and foremost, I would like to thank my supervisor Dr Martin Fronius for providing me with this exciting opportunity to study the effects of shear stress and carbon monoxide on ENaC. The opportunity provided me with hands on experience of the research world and helped me immensely in the development of skill that would prove priceless in life. I am truly grateful for the immense amount of support, guidance and advice from Martin, always putting up with my tardiness. This year has truly been wonderful thanks to Martin!

I would also like to thank all members of the Fronius lab including, Puja Paudel, Vikash Kumar Shah, and Pinky Suman. They provided me with helpful advice throughout my project and helped me transition into the post-graduate life.

I am also immensely grateful of the support from Emily Brown, who provided me with the training and skill I needed to perform TEVC using Roboocyte2. Without her help, this project would've been several magnitudes more difficult.

I'd also like to thank AP Ivan Sammut, and Adam Chau from the pharmacology department for providing me with their carbon monoxide donor and helping me set up the carbon monoxide perfusion equipment. They also provided me with helpful advice and guidance in all things relating carbon monoxide.

I'd also like to thank Leo Van Rens from Emtech and Anne Ryan from the glass blowing unit. They were extremely helpful in helping me make the custom perfusion head for my shear stress protocol, and always putting up with my short-noticed jobs.

Furthermore, I'd like to extend thanks to all members of the Epithelial Journal Club, for the support and guidance in my presentation skills.

I'd like to thank all the friends I have made throughout this year in my honors degree, including Aisya Zamri, Amie Siemonek, Chantelle Leigh Murrell, Cherokee Walters, Chris Veitch, Daniel Lavin, Grace Belworthy, Hiroki Ambalawanar, Ji Woo Kim, Lucas Hinton, Pruthvi Ranganatha, Vasu Signh, Yeri Rim, and Zhean Toñacao. Thank you guys, very much for putting up with me in the office and trying out my weird Asian food!

Last but not least, I'd like to thank Shaojie Zheng, my flatmate and friend in providing me with an immense amount of support throughout this year.

Table of Contents

Abstract ii

Acknowledgements iv

Table of Contents vi

List of Figures ix

List of Tables xi

List of Abbreviations xii

Chapter 1: Introduction 1

1.1 Preface 2

1.2 ENaC 4

1.2.1 Structure 4
1.2.2 Function 7
1.2.3 Regulation 9

1.3 Hypertension 12

1.3.1 Kidneys 12
1.3.2 Vascular Endothelium 13

1.4 Shear Stress 15

1.5 Carbon Monoxide 18

1.6 δβγ-Channels 20

1.7 Aims and Hypothesis 22

1.7.1 Shear Stress 22
1.7.2 Carbon Monoxide 22

Chapter 2: Methods 23

2.1 Methods 24

2.2 *Xenopus laevis* oocytes 26

2.2.1 Oocyte Harvest 26
2.2.2 Oocyte isolation and cultivation 28
2.2.3 cRNA Injection 30

2.3 Two Electrode Voltage-Clamp (TEVC) 32

2.3.1 Roboocyte2 32

2.4 Shear Stress **36**

2.4.1 Shear Force Perfusion Head **36**
2.4.2 Shear Force Calibration **37**
2.4.3 Perfusion Protocol **41**
2.5 Carbon Monoxide **43**

2.5.1 Carbon Monoxide Perfusion system **43**
2.6 Statistical Analysis **45**

Chapter 3: Results **46**

3.1 The Effect of Shear stress on Human Epithelial Sodium Channels **47**

3.1.1 Shear Stress activates αβγ-ENaC **47**
3.1.2 Shear stress activates δβγ-ENaC **49**
3.1.3 δβγ-ENaC is more sensitive to shear stress than αβγ-ENaC **49**
3.1.4 Shear stress effect in *Xenopus* oocytes due to ENaC activation **50**
3.2 The effect of carbon monoxide on human epithelial sodium channels **52**

3.2.1 Carbon Monoxide effect on αβγ-ENaC **53**
3.2.2 Effect of Carbon Monoxide on δβγ-ENaC **58**
3.2.3 The effect of carbon monoxide compared between αβγ-ENaC and δβγ-ENaC **61**

Chapter 4: Discussion **64**

4.1 Overview **65**

4.2 ENaC is activated by shear stress **66**

4.2.1 ENaC responds to shear stress in a dose dependent manner **67**
4.3 Carbon Monoxide and ENaC **68**

4.3.1 Carbon monoxide may have a concentration dependent effect on αβγ-ENaC **68**
4.3.2 Carbon monoxide had no effect on δβγ-ENaC **70**
4.3.3 Comparing the effect of carbon monoxide between αβγ-ENaC and δβγ-ENaC **71**
4.4. Methodological considerations and future directions **71**

4.5 Conclusion and future directions **74**

References **75**

List of Figures

Figure 1: General overview of ENaC structure. 5

Figure 2: The extracellular loop of ENaC. 6

Figure 3: General overview of ENaC function. 8

Figure 4: ENaC-mediated sodium transport regulation. 9

Figure 5: Visual representation of the mechanism of shear stress 15

Figure 6: Endogenous synthesis of carbon monoxide from heme in the human body catalyzed by hemoxygenase. 17

Figure 7: Visualization of stages in *Xenopus laevis* oocyte development. 27

Figure 8: Visualization of cRNA injection procedure. 29

Figure 9: Schematic of Roocyte2 proprietary measuring head assembly. 31

Figure 10: Schematic of Roboocyte2 TEVC System. 32

Figure 11: Sample of Roboocyte2 Scripting. 33

Figure 12: A comparison of the factory perfusion head and the custom perfusion head. 35

Figure 13: Calibration of Laminar Shear Stress to Perfusion Rate. 38

Figure 14: Schematic of carbon monoxide perfusion. 41

Figure 15: Shear Stress activates αβγ-ENaC. 46

Figure 16: Human δβγ-ENaC is activated by Shear Stress. 47

Figure 17: Comparison of half-maximal effective shear stress (EC_{50}) between αβγ-ENaC and δβγ-ENaC. 48

Figure 18: Control experiment for shear stress application. **49**

Figure 19: Representative current traces of αβγ-ENaC expressing oocytes. **52**

Figure 20: Effect of carbon monoxide on αβγ-ENaC expressing oocytes. **53**

Figure 21: t_6/t_0 ratios in αβγ-ENaC expressing oocytes. **54**

Figure 22: Slopes of αβγ-ENaC expressing oocytes. **55**

Figure 23: Representative current traces of δβγ-ENaC expressing oocytes. **56**

Figure 24: Effect of carbon monoxide on δβγ-ENaC expressing oocytes. **57**

Figure 25: t_6/t_0 response to carbon monoxide in δβγ-ENaC. **58**

Figure 26: Slopes of δβγ-ENaC expressing oocytes. **59**

Figure 27: Comparison of t_6/t_0 ratios between αβγ-ENaC and δβγ-ENaC. **60**

Figure 28: Comparison of slopes between αβγ-ENaC and δβγ-ENaC. **61**

List of Tables

Table 1: Components of all solutions used. **24**

List of Abbreviations

µA	Microamperes
µL	Microlitres
µM	Micromolar
µg/mL	Micrograms per Millilitre
A	Ampere
AEC	Animal Ethics Committee
Amil.	Amiloride
au	Arbitrary Unit
Cat. No.	Catalogue Number
Ca^{2+}	Calcium Ion
$CaCl_2$	Calcium Chloride
Cd	Drag Coefficient
cm/s	Centimetres per Second
cm3/s	Centimetres cubed per Second
CO	Carbon Monoxide
cRNA	Complimentary Ribonucleic Acid
CulORi	Culture Oocyte Ringers
D	Diameter
dyn	Dynes

dyn/cm^2	Dynes per centimetres squared
ECM	Extracellular Matrix
EGTA	Ethylene Glycol-bis(β-aminoethyl ether)-N,N,N′,N′-tetraacetic Acid
ENaC	Epithelial Sodium Channel
eNOS	Endothelial Nitric Oxide Synthase
EPA	Environmental Protection Agency
F_{drag}	Effective Drag Force
F_{shear}	Effective Shear Force
g/cm.s	Grams per Centimetre Seconds
g/L	Grams per Litre
HEPES	4-(2-hydroxyethyl)-1-piperazineethanesulfonic Acid
HO	Heme Oxygenase
KCl	Potassium Chloride
M	Mole
$MgCl_2$	Magnesium Chloride
min	Minute
mL	Millilitre
mL/min	Millilitre per Minute
mM	Millimolar
mm	Millimetre
n	Number of Oocytes

N	Number of animals
Na+	Sodium Ions
Na^+/K^+ ATPase	Sodium Potassium ATPase
NaCl	Sodium Chloride
ng	Nanogram
ng/µL	Nanogram per Microliter
nL	Nanolitre
NMDG	N-Methyl-D-glucamine
NO	Nitric Oxide
oCOM-21b	Organic Carbon Monoxide Molecule - 21b
Ori	Oocyte Ringers
Re	Reynolds Number
RNase	Ribonuclease
s	Second
SEM	Standard Error of Mean
SF	Shear Force
t_0	Time 0
t_6	Time 6
TEVC	Two Electrode Voltage Clamp
USA	United States of America
α	Alpha
β	Beta

γ	Gamma
δ	Delta
θ	Density of Water
λ	Kinematic Viscosity of Water
ω	Flow Velocity

1

Introduction

1.1 Preface

Hypertension is a medical condition characterized by chronically elevated blood pressures, potentially causing damage to the arterial walls. This disease affects over a billion people worldwide and is a primary risk factor for cardiovascular diseases, including stroke, and heart attacks. As of currently, there are multiple drugs to treat the condition including ACE-inhibitors, diuretics and beta blockers. But some patients who take a multiple medications to combat the disease are still unable to lower the blood pressure to normal ranges. This raises the need for a better understanding of the disease in order to develop more effective treatments.

ENaC, or otherwise known as epithelial sodium channels are responsible for the passive movement of sodium ions through the apical cell membrane of salt absorbing epithelia. ENaC is composed of multiple subunits, and in humans namely the subunits mainly form αβγ-ENaC, or δβγ-ENaC. αβγ-ENaC has been shown to be responsive to shear stress, a phenomenon that is increased during hypertension. And increased αβγ-ENaC activity has been shown to inhibit vascular relaxation, potentially exacerbating the effects of hypertension. δβγ-ENaC has been found to be expressed in the endothelium of arteries including the aorta. But how the effects of shear stress on δβγ-ENaC compares to αβγ-ENaC is currently unclear. Therefore, a better understanding on how δβγ-ENaCs respond to elevated shear stress such as during hypertension, may potentially allow us to better understand the disease.

On the other hand, carbon monoxide is under research in the treatment of cardiovascular diseases. And furthermore, carbon monoxide has also been shown to have an inhibitory effect on αβγ-ENaC. However, how carbon monoxide affects δβγ-ENaC is currently unknown, but a better understanding here may place carbon monoxide as a potential therapeutic in the treatment of hypertension.

Therefore, we will aim to compare how these two ENaCs respond to shear stress, as well as their response to carbon monoxide.

1.2 ENaC

Epithelial sodium channels are members of the ENaC/Degenerin Superfamily of proteins (Canessa *et al.*, 1994). ENaC are predominantly found on the apical membrane of the epithelial lining of the kidney (Hager *et al.*, 2001) and the lungs (Enuka *et al.*, 2012). ENaC facilitates the passive movement of sodium ions (Na^+) into the tissue (Hanukoglu & Hanukoglu, 2016). This results in a net movement of sodium ions into the tissue, increasing the solute concentration within the tissue. This creates an osmotic gradient, driving water uptake via osmosis (Hanukoglu & Hanukoglu, 2016). Therefore, ENaC plays a major role water homeostasis and blood pressure regulation (Pratt, 2005; Sharma *et al.*, 2017).

1.2.1 Structure

Structurally, ENaC is a heterotrimer, and is composed of three homologous subunits of either alpha (α), beta (β), gamma (γ), or delta (δ) subunits (Canessa *et al.*, 1994). And it was only until recently that ENaC was confirmed to be a trimer (Noreng *et al.*, 2018), as ENaC's stoichiometry was heavily debated prior (Shobair *et al.*, 2016).

In humans, ENaC is most commonly found to be composed of α, β, and γ subunits. These will be hence be referred to as αβγ channels (Fig. 1A). Because they are the predominant combination found in epithelia, most studies have been focused around this configuration of subunits. There is another combination of subunits of significant interest and is composed of δ, β, and γ subunits and will hence referred to as δβγ-ENaC

(Fig. 1B). These have been less well studied as they are only found in humans and not rats (Giraldez *et al.*, 2012).

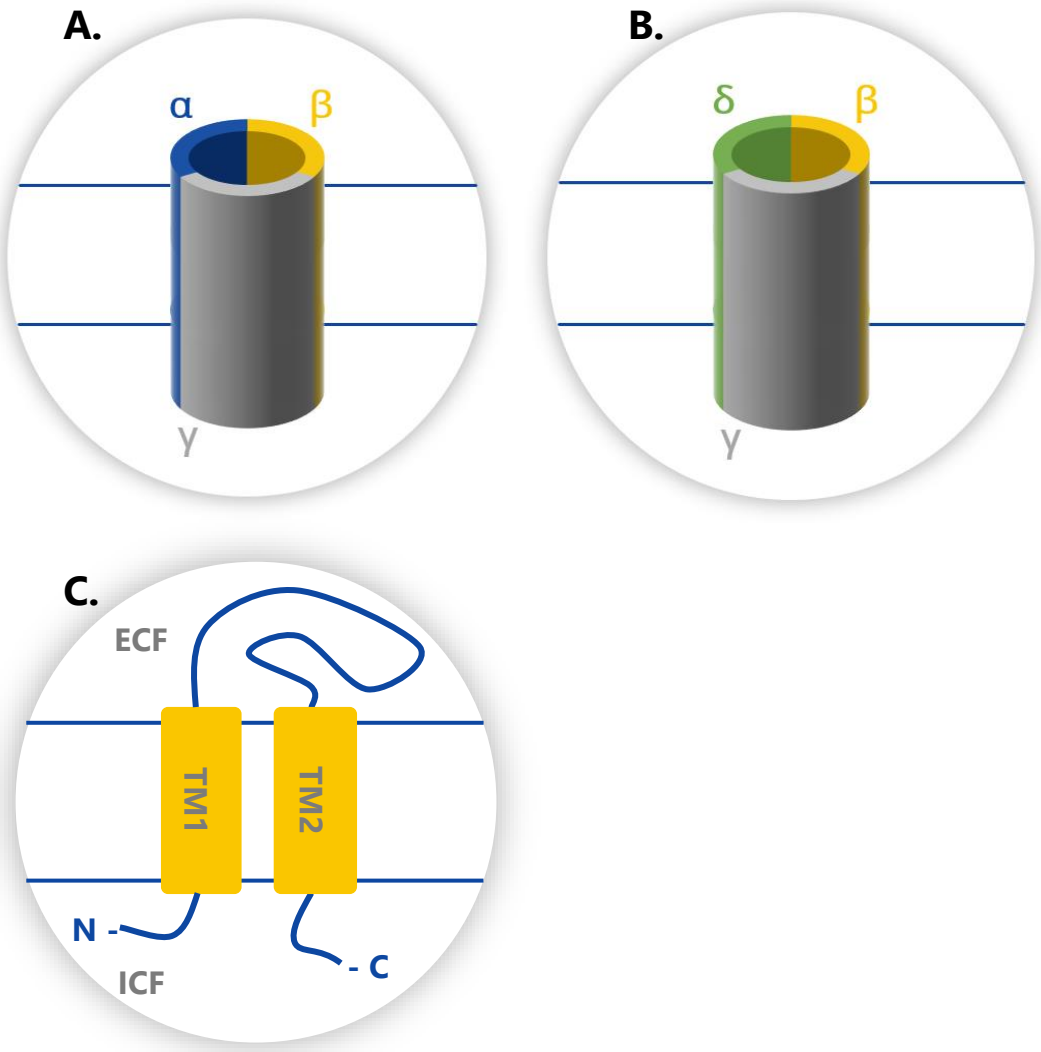

Figure 1: General overview of ENaC structure.
A. General structure of αβγ channels, composed of three subunits forming a pore like structure. **B.** General structure of δβγ channels also forming a pore like structure. **C.** Basic ENaC subunit structure including two transmembrane domains and a long extracellular loop. The C and N-termini are found in the cell interior.

As mentioned earlier, ENaC proteins are members of the ENaC/degenerin superfamily (Canessa *et al.*, 1994). Members of this superfamily exhibit stereotypical structural

features including a large extracellular loop found between two transmembrane domains, with short intracellular C- and N- termini (Canessa *et al.*, 1994; Kashlan & Kleyman, 2011) (Fig. 1C). In humans, the structure of the extracellular loops is similar between each ENaC subunit (Kashlan & Kleyman, 2011). But, the structures of the C- and N- termini of ENaC has yet to be determined.

The extracellular domain in ENaC exhibit characteristic regions including β-ball, finger, knuckle, palm and thumb domains that are connected to their transmembrane domains via a wrist region (Noreng *et al.*, 2018) (Fig. 2). A further region of interest is the GRIP (Gating Relief of Inhibition by Proteolysis) domain, which has been elucidated to play a role in the gating of ENaC (Noreng *et al.*, 2018).

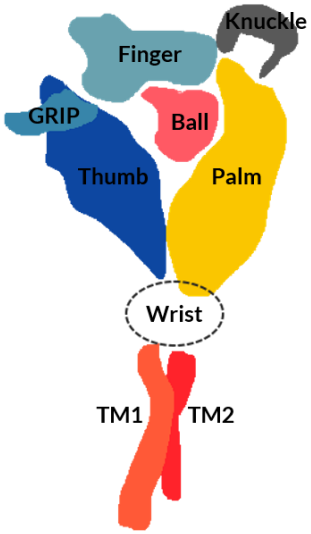

Figure 2: The extracellular loop of ENaC.
A visual representation of the extracellular loop, showing the Ball, Finger, GRIP, Knuckle, Thumb, Palm and Wrist region connected to the two transmembrane domains.

1.2.2 Function

ENaC in general, provides a passage for the passive movement of sodium ions into the cell, down its electrochemical gradient, and is the rate limiting step for sodium uptake. The electrochemical gradient is driven by a basolateral sodium potassium ATPase pump (Na^+/K^+-ATPase), pumping out three sodium ions in exchange for 2 potassium ions. The potassium ions are recycled out of the cell passively, via a basolateral potassium channel (Garty & Palmer, 1997). This causes a net movement of sodium ions into the tissue, increasing the tissues solute concentration, creating an osmotic gradient (Palmer & Andersen, 2008) (Fig. 3). Therefore, water is driven into the tissue down its osmotic gradient, resulting in net water absorption (Palmer & Andersen, 2008).

It has been shown that the α subunit alone can facilitate the movement of sodium ions through the cell membrane (Canessa *et al.*, 1994). However, only upon coexpression with both beta and gamma subunits does sodium transport increase 100-fold compared to the α subunit alone (Canessa *et al.*, 1994). A similar phenomenon is seen with the δ subunit, where the δ subunit alone can facilitate sodium movement, however, coexpression with beta and gamma subunits increases sodium transport 2-fold (Haerteis *et al.*, 2009). Furthermore, δβγ-ENaC produces amiloride sensitive currents that are 11 times that of αβγ-ENaC (Haerteis *et al.*, 2009).

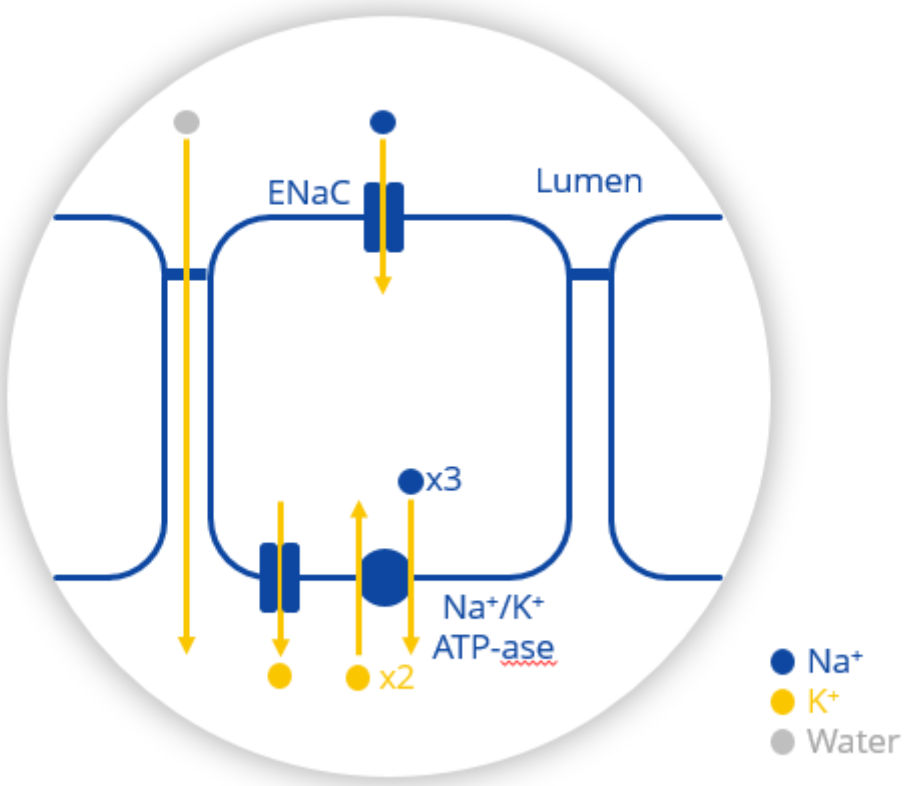

Figure 3: General overview of ENaC function.
Where blue dots represent sodium ions, yellow dots potassium ions and the grey dots as water. Basolateral sodium potassium pump provides electrochemical gradient for sodium resorption through ENaC. Net flow of sodium causes solute concentration to increase within the tissue, resulting in water uptake through both the transcellular pathway and paracellular pathway.

ENaC is also amiloride sensitive. Upon amiloride administration, ENaC mediated sodium transport is reduced by blockage of the ENaC pore, restricting ion access through the channel (Canessa *et al.*, 1993). This reduces the open probability of ENaC which will be discussed further in the regulation section. The mechanism behind this effect was shown to be a direct blockage of the ENaC pore by amiloride, preventing Na^+ passage (Palmer, 1984). This amiloride sensitive characteristic of ENaC has been vital in the research and understanding of ENaC activity. Its perfusion during electrical

recordings allows the determination of amiloride sensitive current, the current that is attributed to ENaC.

1.2.3 Regulation

ENaC is a constitutively active channel, meaning it is always active when inserted into the cell membrane (Garty & Palmer, 1997). But ENaC mediated sodium transport (I) may be modulated in two ways (Fig. 4). Either by altering the open probability of the channel or changing the surface expression (N) of the channel. Both ways can result in changes to sodium transport, however, modulating the open probability generally leads to an acute effect when compared to modulating the surface expression. This is because it requires time to synthesize more ENaC.

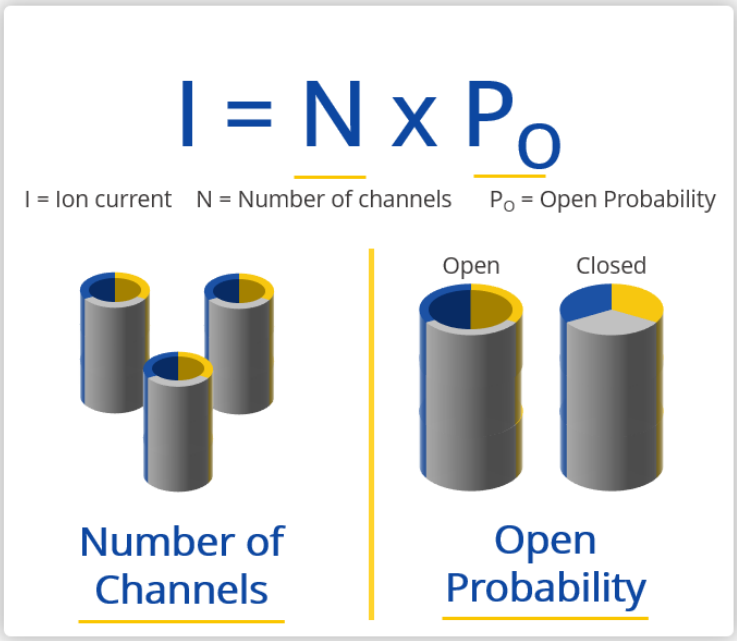

Figure 4: ENaC-mediated sodium transport regulation.
General graphical representation of ENaC activity (I) regulation via either altering the surface expression (number of channels) (N) or the open probability (P_o).

1.2.3.1 Open Probability

The open probability (P_o) of ENaC is the probability that the channel is open in any point in time. By altering this open probability, the net movement of sodium ions can be modulated, and hence the net water movement may change as well. Open probability has been shown to be modulated via many factors, including extracellular sodium concentrations (Fuchs *et al.*, 1977), pH (Chalfant *et al.*, 1999), and proteases (Kleyman *et al.*, 2009). Importantly, the open probability of ENaC has been shown to be modulated by shear stress (Althaus *et al.*, 2007) and will be discussed in detail in the shear stress section.

1.2.3.2 Surface expression

The surface expression of ENaC, or the number of ENaC found on the surface of the cell membrane may also be altered to modulate ENaC mediated sodium transport activity. This requires a careful balance between ENaC internalization (Ubiquitination) from the membrane and insertion (Aldosterone) into the membrane.

ENaC contains a proline rich sequence called the PY motif found in the cytoplasmic C-terminal region of ENaC subunits (Schild *et al.*, 1996; Staub *et al.*, 1996). Here, Nedd4-2, a ubiquitin-protein ligase binds and adds a ubiquitin tag to it (ubiquitination), marking ENaC for internalization and breakdown (Harvey *et al.*, 1999; Kamynina *et al.*, 2001; Malik *et al.*, 2005). This results in a reduced surface expression of ENaC.

Aldosterone, a hormone, promotes the increased abundance ENaC in the cell surface when blood volume is sensed to be low. Aldosterone is released by the adrenal gland to increase blood volume, pressure and to maintain extracellular sodium

concentrations (Bollag, 2011). Aldosterone binds to mineralocorticoid receptors, activating serum glucocorticoid kinase 1 (SGK). SGK1 in turn phosphorylates ubiquitin-protein ligase Nedd4-2. Preventing Nedd4-2 from acting on ENaC for internalization (Debonneville *et al.*, 2001). This reduced internalization results in increased surface expression of ENaC.

1.3 Hypertension

Hypertension is a chronic medical condition where blood pressure in the arteries is persistently elevated above normal ranges (NHLBI, 2018). Having a high blood pressure itself does not result in immediate consequences for the patient. However, chronic hypertension is a major risk factor in cardiovascular diseases including stroke and heart failure (NHBLI, 2018).

Blood pressure is affected by total cardiac output, and total peripheral resistance. Importantly in relation to ENaC, blood pressure may be modulated through total blood volume (Kidneys) (Evans & Bie, 2015), affecting the cardiac output and arterial stiffness (Endothelium) which affects the total peripheral resistance (Perez *et al.*, 2009).

1.3.1 Kidneys

As mentioned previously, ENaC mediated sodium transport drives water uptake (Palmer & Andersen, 2008). This novel function of ENaC mediated sodium transport puts ENaC in an important position in water homeostasis, which influences blood volume. This is particularly true in the kidneys where ENaC is found in abundance along the epithelium of the distal nephron to aid in water resorption from the glomerular filtrate (Rossier *et al.*, 2013). And therefore, a disturbance in its activity may lead disrupted water homeostasis, and hence altering blood volume (Rossier, 2014).

A well-known disease that results in hypertension from ENaC malfunction in the kidneys is Liddle's syndrome (Schild, 1996). Liddle's syndrome is a rare genetic disorder where the PY-motif of ENaC has obtained gain-of-function mutations (Schild *et al.*,

1995; Schild *et al.*, 1996). This prevents the binding of Nedd4-2 to ENaC to undergo ubiquitination, resulting in reduced internalization of ENaC on the cell surface, meaning there is a greater abundance of ENaC expressed (Schild *et al.*, 1995; Schild *et al.*, 1996). As stated earlier, ENaC-mediated sodium transport can be modulated via surface expression. And therefore, an increased surface abundance of ENaC results in increased sodium resorption, increased water resorption and increased blood volume. This ultimately raises the blood pressure of the patient resulting in severe hypertension (Snyder *et al.*, 1995; Firsov *et al.*, 1996).

As of currently treatments for this disease includes a reduced sodium diet and amiloride administration. These treatments combined reduces ENaC-dependent sodium absorption in the kidneys and hence reduced water resorption, bringing blood volume and pressure back towards normal.

1.3.2 Vascular Endothelium

Contrary to its name, ENaC has been shown to be found in non-epithelial tissues as well. ENaC has been previously been shown to be present in microvascular endothelium (Chen *et al.*, 2004; Wang *et al.*, 2009), and unpublished data from the Fronius lab has also found evidence of its presence in human arteries, likely in the endothelium.

ENaC in vascular endothelium has been shown to play a role in affecting vascular relaxation via endothelial Nitric Oxide Synthase (eNOS) (Perez *et al.*, 2009). eNOS in arteries is an enzyme that catalyzes the synthesis of nitric oxide (NO), a small gaseous molecule that has a role in many biological processes (Sessa, 2004). Importantly, NO

produced by eNOS in the vascular endothelium is an important regulator of vascular relaxation. This is because NO inhibits voltage gated Ca^{2+} channels in vascular smooth muscle, reducing the cytosolic Ca^{2+} concentration (Bolotina *et al.*, 1994). This reduction in Ca^{2+} ions prevents contraction of the vascular smooth muscle, resulting in vasorelaxation (Horowitz *et al.*, 1996). This reduces the total peripheral resistance, hence reducing blood pressure.

However, ENaC mediated sodium transport has been shown to be an inhibitor of eNOS activity (Perez *et al.*, 2009). This causes reduced NO synthesis and hence reduced vascular smooth muscle relaxation, resulting increased total peripheral resistance and blood pressure. This suggests ENaC influences the development of hypertension in more ways than just one.

1.4 Shear Stress

Shear stress is a physical phenomenon where a passing flow of fluid such as blood in the arteries exerts frictional forces against the surrounding tissue, such as the endothelium in arteries (Fig. 5). This causes a mechanical deformation of the tissue and may lead to activation of mechanosensitive components found on the membrane of the tissue.

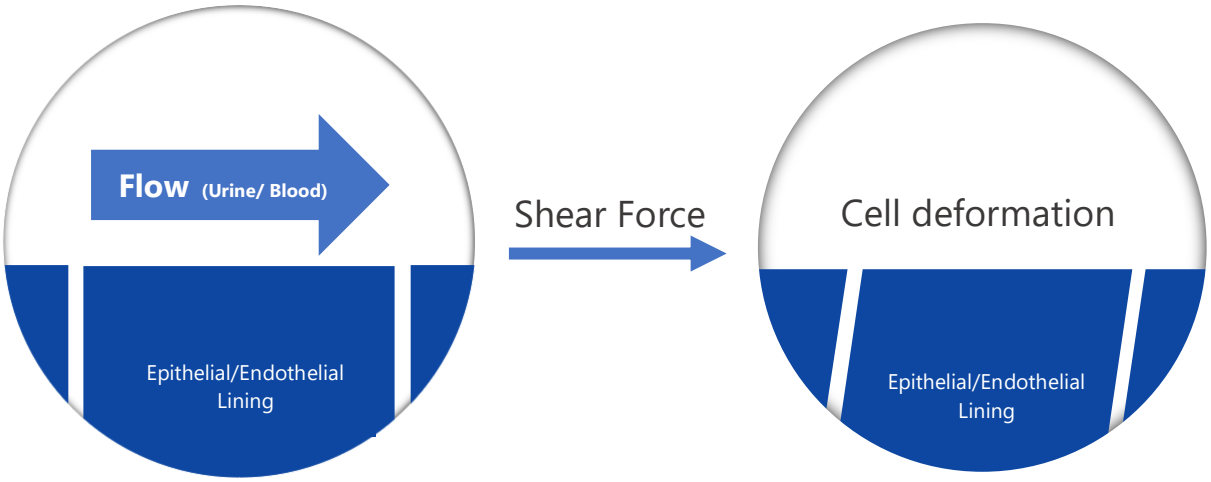

Figure 5: Visual representation of the mechanism of shear stress
Visual representation of how shear stress causes deformation of the epithelial/endothelial lining. The passing flow of fluid causes physical deformation and stretch of the tissue lining.

ENaC has been shown previously to be mechanosensitive to shear stress (Althaus *et al.*, 2007; Fronius *et al.*, 2010). And studies done using Rat and Xenopus αβγ-ENaC have indicated that αβγ-ENaC responds to shear stress in a dose dependent manner (Carattino *et al.*, 2004; Althaus *et al.*, 2007). The studies showed that an increase in shear stress resulted in upregulation of αβγ-ENaC open probability, which increases ENaC-mediated sodium transport (Althaus *et al.*, 2007; Carattino *et al.*, 2007).

The exact mechanism behind this phenomenon is not well understood and two models were proposed. The bilayer model, where channels are gated by membrane deformation as a result of shear stress administration (Hamill & Martinac, 2001). And the tethered model, where mechanical forces are transduced to the channel through a tether attached to either the intracellular and/or extracellular matrix (Hamill & Martinac, 2001). Unfortunately, neither model has convincing evidence to support them. Carattino *et al.* (2007) found that altering properties of the lipid membrane resulted in no change to the ENaC response to shear stress, disproving the bilayer model. And the tethered model was disproven in a study where activation of ENaC via shear stress was not affected when the actin cytoskeleton was disrupted (Karpushev *et al.*, 2010).

As of currently, it is proposed that the extracellular loops are involved in this mechanical activation (Althaus *et al.*, 2007). A study found that upon proteolytic cleavage of the extracellular loops, different response to shear stress were seen in different orthologs (Althaus *et al.*, 2007). This is further supported by another study where mutations at selected sites within the loop altered the magnitude of ENaC activation in response to shear stress (Shi *et al.*, 2011). Further studies are needed to confirm the exact mechanism behind the shear stress induced ENaC effect.

However, regardless of its mechanism, in hypertension where blood flow is increased, ENaC found along the endothelium lining will be exposed to increased levels of shear stress, resulting in its upregulation of ENaC mediated sodium transport. And as stated previously, this in arteries will result in inhibited vascular relaxation (Perez *et al.*, 2009), potentially exacerbating the effects of hypertension.

1.5 Carbon Monoxide

Carbon monoxide is commonly known as a colourless, odourless gas that upon inhalation in high concentrations results in suffocation. Carbon monoxide exerts its toxic effects by strongly binding to the iron atoms of heme. This binding prevents oxygen uptake, and hence impedes oxygen transport. Prolonged exposure to this toxic gas results in tissue hypoxia and ultimately, death (Piantadosi, 2002; Gorman *et al.*, 2003). Because of these deadly characteristics of the diatomic molecule, research into its presence in the human physiology has been delayed until recently, where the gas has been found to function as a gasotransmitter in the human body (Verma *et al.*, 1993).

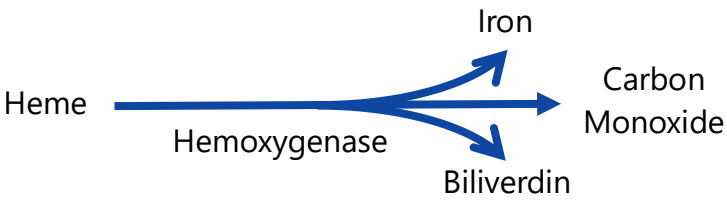

Figure 6: Endogenous synthesis of carbon monoxide from heme in the human body catalyzed by hemoxygenase.
The breakdown of heme is catalysed by Hemoxygenase where it forms iron, biliverdin and carbon monoxide.

Carbon monoxide is endogenously synthesized in the human body via the oxidation of heme, where biliverdin and iron are also produced as byproducts (Maines, 1997) (Fig. 6). This reaction is catalysed by the enzyme hemoxygenase (HO), and two isoforms are found in the human body, an inducible HO-1 isoform and a constitutive HO-2 isoform (Maines, 1997). Both isoforms are expressed in many tissues around the human body, particularly in the vascular endothelium (Zakhary *et al.*, 1996) and smooth muscle cells

(Ewing *et al.*, 1994). Of course, carbon monoxide may also be exogenously administrated through direct gas inhalation, or in a more clinically relevant form that allows precise dosing, carbon monoxide releasing molecules (CORMS). However, due to the metal carbonyl structure of CORMs, CORMs typically present as a long term health risk (Foresti *et al.*, 2008; Garcia-Gallego & Bernardes, 2014). Therefore, there is currently research in organic CORMs that are non-metallic, which is less toxic than traditional CORMs (Abeyrathna *et al.*, 2017).

These carbon monoxides releasing molecules are important, as carbon monoxide is currently under development as a drug for cardiovascular diseases because carbon monoxide has been shown to influence smooth muscle proliferation (Morita *et al.*, 1997; Song *et al.*, 2002) and platelet aggregation (Brune & Ullrich, 1987; Chlopicki *et al.*, 2012). But perhaps most importantly in relation to this project, carbon monoxide has been shown to influence ENaC activity. It has been shown that upon application of carbon monoxide in the form of CORM-3. ENaC-mediated Na transport is inhibited in a dose response fashion. And this effect likely affects the open probability of ENaC as treatment with cell trafficking inhibitors resulted in no change of the ENaC response to carbon monoxide (Althaus *et al.*, 2009).

However, it has also been shown that carbon monoxide is able to increase ENaC-mediated Na transport, also via increasing open probability (Wang *et al.*, 2009). These conflicting results may suggest a tissue specific mechanism of carbon monoxide as the inhibitory response was seen in alveolar type 2 cells (Althaus *et al.*, 2009), whereas the activation response was seen in cells of the kidney cortical collecting duct (Wang *et al.*,

2009). As there are currently only these two studies on the effect of carbon monoxide on ENaC, the exact effect of carbon monoxide is uncertain. However, grasping a better understanding of the effect, may potentially pose carbon monoxide as a potential therapeutic in the treatment of hypertension. This is because as stated earlier, ENaC is upregulated by shear stress (Althaus *et al.*, 2007), and upregulated ENaC activity leads to inhibition of vascular relaxation (Perez *et al.*, 2009), which potentially exacerbates the effect of hypertension. Therefore, the use of carbon monoxide as a potential inhibitor of ENaC may prevent the inhibition of vascular relaxation, alleviating some effects of hypertension.

1.6 δβγ-Channels

Up to now, all data presented in terms of shear stress and carbon monoxide etc. has only been tested in αβγ-ENaC. Therefore, little is known about δβγ-ENaC including its response to carbon monoxide. The lack of studies likely arises due to it being not expressed in mice (Giraldez *et al.*, 2012), and has only recently been discovered.

As the name implies, unlike αβγ-ENaC, δβγ-ENaC contain a δ subunit instead of an α subunit. And as stated earlier, the δ subunit alone is also capable of sodium transport, and sodium transport activity is greatly enhanced by forming an amiloride sensitive heterotrimer with β and γ subunits (Haerteis *et al.*, 2009). But as the δ subunit on shares 34 % gene identity with the α subunit (Hanukoglu & Hanukoglu, 2016), differences in function are to be expected.

Functionally, δβγ-ENaC has been shown experimentally to have an 11-fold higher open probability and hence greater sodium conductance when compared to αβγ-ENaC (Haerteis *et al.*, 2009). Also, δβγ-ENaC have a greater affinity for sodium ions over lithium ions, unlike αβγ-ENaC (Canessa *et al.*, 1994).

δβγ-ENaC are also expressed in different tissues when compared to αβγ-ENaC which are highly expressed in salt-absorbing epithelia. Instead, δβγ-ENaC are highly expressed in the parts of the brain, heart, liver, pancreas, skeletal muscle, and to a smaller degree, regions of the kidney (Waldmann *et al.*, 1995; Yamamura *et al.*, 2004). But most importantly, unpublished data from the Fronius lab has found δβγ channels presence in the endothelium of human arteries, therefore it may potentially also play a role in ENaC-mediated inhibition of vascular relaxation. This is of particular relevance as it has been shown δβγ-ENaC also responds so shear stress (Abi-Antoun *et al.*, 2011). But whether this response is also dose-dependent and how it compares to the response seen in αβγ-ENaC is still unknown.

Therefore, a better understanding of how δβγ channels responds to shear stress, may provide a better understanding of hypertension. And furthermore, a better understanding of how δβγ channels respond to carbon monoxide may pose carbon monoxide as a potential therapeutic in the treatment of hypertension.

1.7 Aims and Hypothesis

1.7.1 Shear Stress

Based on current knowledge of ENaC, it is well known that both αβγ-ENaC and δβγ-ENaC is responsive to shear stress, but how the response compares between the two types of ENaC is unknown. Given that δβγ-ENaC has been shown to have a higher open probability than αβγ-ENaC. I hypothesize that a dose-dependent response to shear stress will be seen in both αβγ-ENaC and δβγ-ENaC, and the response is greater in δβγ-ENaC.

Aim: Compare how the shear stress response is different between human αβγ-ENaC and δβγ-ENaC.

1.7.2 Carbon Monoxide

There is currently sparse literature on the effect of carbon monoxide on ENaC, with only two articles describing conflicting effects in αβγ-ENaC. However, it is clear that carbon monoxide does influence ENaC activity in some way. Therefore, I hypothesize carbon monoxide causes an inhibitory response in both αβγ-ENaC and δβγ-ENaC, with a greater response in δβγ-ENaC.

Aim: Identify the effects of carbon monoxide on both αβγ-ENaC and δβγ-ENaC, and how they compare between the two types of ENaCs.

2

Methods

2.1 Methods

Oocytes from *Xenopus laevis* were used to express the ENaC channels of interest. And by applying increasing levels of shear stress and oCOM-21b, the resulting effects on ENaC mediated sodium transport were assessed using Two Electrode Voltage Clamping (TEVC). The composition of all solutions used in this project can be found in table 1 below:

Table 1: Components of all solutions used.

Components	Units	CulORi	ORi	Ca^{2+} free ORi	NMDG	Amiloride-containing ORi
NaCl	mM	90	90	90	10	90
KCl	mM	1	1	1	1	1
$CaCl_2$	mM	2	2	-	2	2
HEPES	mM	5	5	5	5	5
$MgCl_2$	mM	-	-	1	-	-
Na^+-Pyruvate	mM	2.5	-	-	2.5	-
NMDG	mM	-	-	-	80	-
EGTA	mM	-	-	1	-	-
Amiloride	mM	-	-	-	-	100
Penicillin	mM	0.06	-	-	0.06	-
Streptomycin	mM	0.02	-	-	0.02	-
Tetracycline	µg/mL	50	-	-	50	-

Legend Table 1: µg/mL = micrograms per microliter; Ca^{2+} = Calcium ion; $CaCl_2$ = Calcium Chloride; CulORi = Culture Oocyte Ringers; EGTA = ethylene glycol-bis(β-aminoethyl ether)-N,N,N′,N′-tetraacetic acid; HEPES = 4-(2-hydroxyethyl)-1-piperazineethanesulfonic Acid; KCl = Potassium Chloride; $MgCl_2$ = Magnesium Chloride; mM = millimolar; Na^+-Pyruvate = Sodium Pyruvate; NMDG = N-Methyl-D-glucamine ; Ori = Oocyte Ringers.

2.2 *Xenopus laevis* oocytes:

We used oocytes from the South African clawed frog, *Xenopus laevis* as the cell model due to their large single cell size, allowing ease of manipulation in TEVC. We heterologously expressed αβγ channels and δβγ channels in these oocytes using cRNA encoding either channel. It is important to note the import and containment of the frogs were approved by the Environmental Protection Authority (EPA approval number: NOC100153). And the harvesting of oocytes approved by the University of Otago's Animal Ethics Committee (AEC approval number: 83-16).

2.2.1 Oocyte Harvest:

Firstly, the oocytes were harvested from the frogs in order to be used in experimentation. Under normal circumstances, the oocytes would be harvested via surgery, with time allotted between surgeries for the recovery of the animals, and up to 3 surgeries per frog. However, as all frogs have already undergone all 3 permitted surgeries, the oocytes used in this experiment were obtained after euthanasia of the animal. All procedures were recorded accordingly in the animal register located next to each tank and clean gloves were worn throughout the handling of frogs and oocytes.

To perform euthanasia, the frog was placed under anaesthesia via submersion in water containing Tricaine Methane Sulfonate (MS-222, Aldrich, Cat.No. E10521-50G) (1.3 g/L, pH 7.4) for 10-15 minutes. Successful anaesthesia was then confirmed via the pedal and righting reflexes. The pedal reflex was confirmed by gently pulling the leg of the frog away from its body, if retraction was observed, anaesthesia has not taken place.

The righting reflex was confirmed by flipping the frog over on to its dorsal side, if the frog attempts to correct itself back into the upright position, anaesthesia has not taken place. An anaesthetized frog suitable for oocyte collection will not exhibit the above reflexes.

After successful anaesthesia was confirmed, the frog was transferred onto a custom-built guillotine, where a stainless-steel rod punctures through the animal's neck, resulting severance of the spinal cord, hence death. Death is further confirmed via insertion of a thin metal probe into the spinal column to further destroy the spinal column.

Following euthanasia, using sharp scissors, a small vertical incision was made in between the midline and the lateral aspect of the abdomen just above the groin. Scissors were then used to cut through the muscular layer to where the ovarian lobes are located. The ovarian lobes were then externalized with forceps and cut off and placed into culture oocyte ringer's solution (CulORi) for storage. The animal was then placed in a sealed bag and disposed of appropriately in a designated freezer. It is important to note the equipment used during each procedure were disinfected using 1% Virkon.

2.2.2 Oocyte isolation and cultivation

Oocytes were then separated from the ovarian lobes into single oocytes via both physical and enzymatical processes. The extracted ovarian lobes were first placed into a clean 100 mm x 20 mm petri dish (Corning, New York, USA) containing CulORi, and each lobe physically torn apart using two thin-headed forceps. Thin-headed forceps were used in this procedure to minimise damage to the oocytes.

Following this, we performed enzymatic defolliculation of the oocytes. The oocytes were transferred into a new clean 100 mm x 20 mm petri dish (Corning, New York, USA) containing CulORi with collagenase (Nordmark, Cat. No. S1746502) added (1.5 mg/mL). The plates were then sealed using parafilm and placed on a platform rocker (Select Bioproducts, NJ, USA) for an incubation period of 90 minutes at 80 RPM. Oocytes were then rinsed three times in CulORi before being transferred into a 50 mL conical bottom tube (Grenier Bio-One, Frickenhausen, Germany) with Ca^{2+} free oocyte solution (Ca^{2+} free ori) for 15 minute incubation whilst being rotated using a rotator (Thermo Scientific, PA, USA).

After this treatment, the now singular oocytes are transferred into another 100 mm x 20 mm petri dish (Corning, New York, USA) containing CulORi for sorting. Fully-grown, undamaged and healthy-looking stage V-VI oocytes (Fig. 7) were selected and stored individually in a 96-well plate, each well containing 200 µL N-Methyl-D-Glucamin CulORi (NMDG) for cRNA injection. Or, sorted oocytes were placed into a separate clean petri dish containing CulORi for storage. Both were incubated in a low temperature incubator (Jeio Tech, Seoul, South Korea) at 17°C for storage.

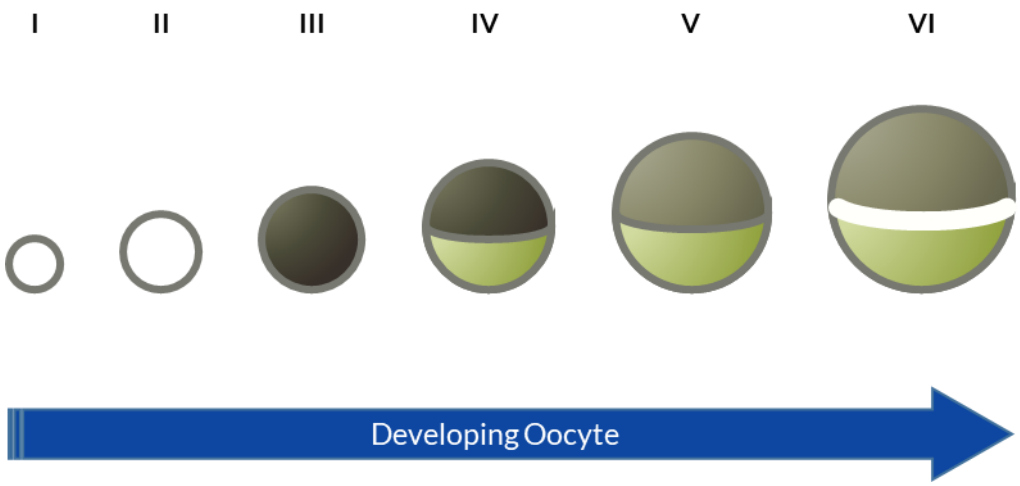

Figure 7: Visualization of stages in *Xenopus laevis* oocyte development.
The development of *Xenopus laevis* oocytes ranges from youngest (Stage I) to most mature (Stage VI) before maturing into fertilization competent eggs. Only oocytes at stage V and VI were selected for cRNA injection.

2.2.3 cRNA Injection

cRNA encoding human α, δ, β, and γ subunits was provided by the Fronius Lab. These were stored in –80 ^{o}C freezers in both single subunit and mixed aliquots. The mixed aliquots of αβγ-ENaC and δβγ-ENaC had equimolar concentrations of each subunit i.e. α:β:γ and δ:β:γ were 1:1:1.

After defrosting the cRNA, aliquots of cRNA encoding αβγ-ENaC and δβγ-ENaC were placed into separate .5 µL Non-stick, RNAse free microcentrifuge tubes (Invitrogen, California, USA) for use in injection. The injection process involved an automated high throughput system, Roboinject (Multichannel systems, Reutlingen, Germany). This system allows precise injection of each oocyte in the 96 well plate with the programmed amount of solution (Fig. 8). Here, oocytes were injected with 20 nL of 11.25 ng/µL cRNA encoding either αβγ-ENaC or δβγ-ENaC. Water controls were also injected with 20 nL of RNAse free water to control for the injection process. In summary, three groups of oocytes result from this injection process, αβγ-ENaC injected oocytes, δβγ-ENaC injected oocytes, and water-injected oocytes as shown in Figure 8 below.

Following injection, the injected oocytes were incubated in the low temperature incubator at 17 ^{o}C over 24-72 hours.

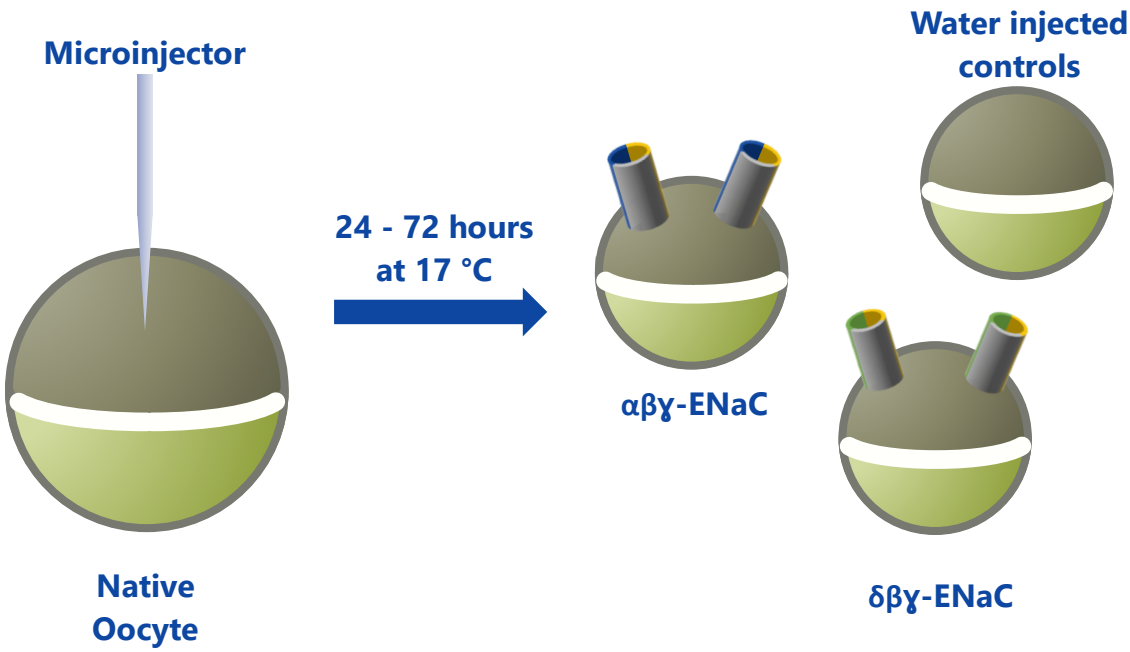

Figure 8: Visualization of cRNA injection procedure.
The oocytes in a 96 well plate was injected using Roboinject system. 2.25 ng of cRNA encoding either αβγ channels or δβγ channels were injected. 20 nL of RNAse free water was injected into water control oocytes.

2.3 Two Electrode Voltage-Clamp (TEVC)

Two Electrode Voltage-clamping (TEVC) was used to assess the effects of shear stress and carbon monoxide on ENaC expressing oocytes. TEVC is a well-established technique in which the cell is artificially held at a set membrane potential, and changes in membrane current can be recorded. This is particularly useful in measuring ion channel activity due to the charged nature of ions.

TEVC involves a total of 4 electrodes, two bath electrodes, a voltage electrode to measure membrane potential, and finally a current electrode which passes electrical current into the cell to control the membrane potential.

2.3.1 Roboocyte2

Roboocyte2 (Multichannel systems, Reutlingen, Germany) is an automated high throughput system used to perform TEVC on *Xenopus laevis* oocytes. This system is composed of the Roboocyte2 (Multichannel systems, Reutlingen, Germany), the robot itself to perform TEVC as well as a fluid perfusion system to control perfusion of fluids, Roboflow (Multichannel systems, Reutlingen, Germany). A computer was used to run Roboocyte2s proprietary software for recording of the electrical activity, as well as the control and scripting of the robot.

In the Roboocyte2 system (Fig. 10), the 4 electrodes required for TEVC, along with the perfusion tubes are incorporated into a single measuring head that is proprietary to the system (Fig. 9). The proprietary measuring microelectrodes (chlorided silver wires) were placed in the glass capillaries of the supplied measuring head, backfilled with 3 M KCl. The bath electrodes were also proprietary chlorided silver wires and submerged directly into the bath solution.

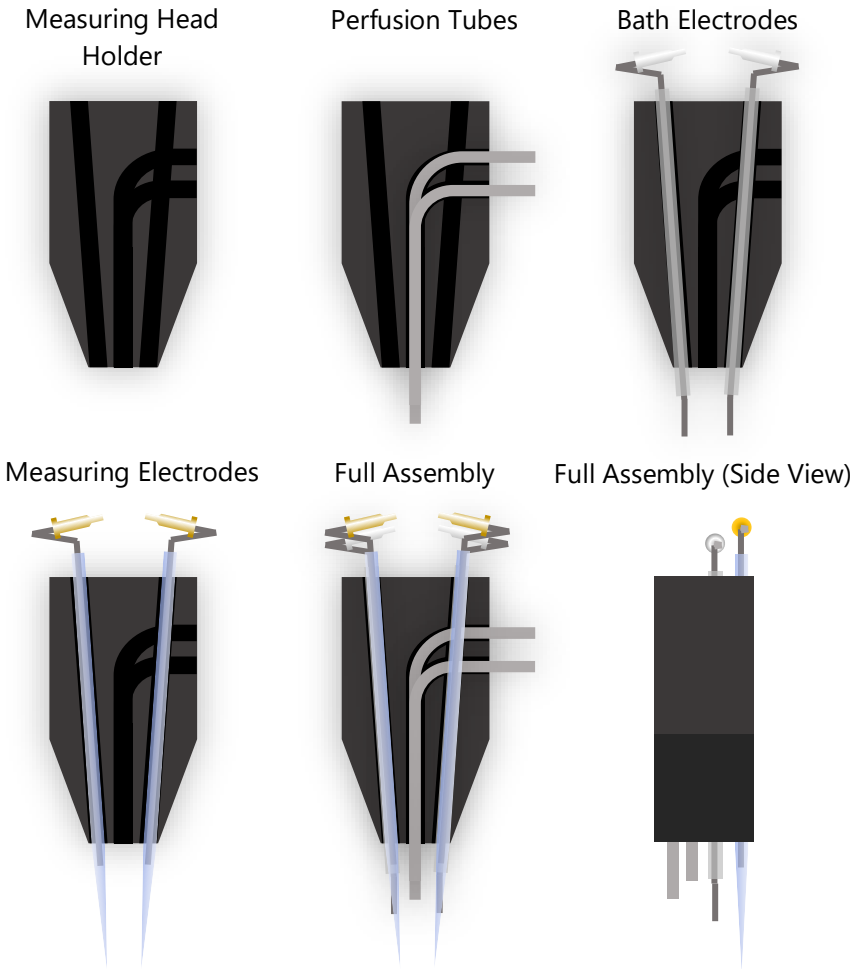

Figure 9: Schematic of Roocyte2 proprietary measuring head assembly.
Roboocyte2 uses a proprietary measuring head, incorporating measuring electrodes, bath electrodes as well as perfusion tubes into a single unit.

The system also incorporates a peristaltic pump to drive the perfusion of the recording well, as well as a separate peristaltic pump to remove excess solution from the recording chamber. The speed of each pump can be modulated individually.

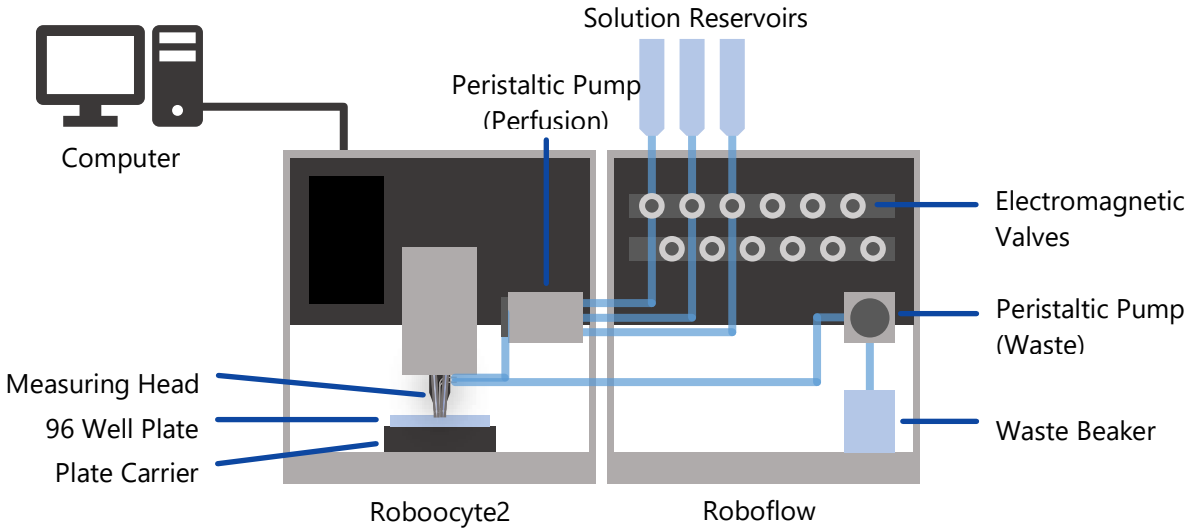

Figure 10: Schematic of Roboocyte2 TEVC System.
The Roobocyte2 system is linked to Roboflow for solution perfusion in each well. Roboflow allows attachment of up to 12 solution reservoirs and may be individually controlled via electromagnetic valves. The perfusion tubes from each reservoir is linked to a peristaltic pump that drives the perfusion of the recording chamber. A separate peristaltic pump removes excess solution from each well into a waste beaker. Roboocyte2 holds the 96 well plate on a plate carrier that moves on the platform via a cushion of air. The plate carrier moves the plate so the well of interest is directly under the measuring head. The positioning of the measuring head and plate carriers are calibrated initially using a specialised microscope and calibration tool.

Using the supplied software, scripts can be written to automate each perfusion protocol as well as the recording process.

2.3.3.1 Roboocyte2 Scripting

As Roboocyte2 is an automated system, scripting was needed to ensure the correct events occurred at the right time. The syntax used in the Roboocyte2 system is a Javascript based language and allows fine control over the recording procedure of each experiment. In general, the script first defines variables and checks the parameters before running the oocyte loop.

The oocyte loop is a section of code that is responsible for the recording of each oocyte. It begins by compensating the electrode DC voltage offsets at each electrode, before testing those in the bath solution. Afterwards, the measuring electrodes impale the oocyte, and measures the membrane potential. Here the script will decide whether impalement was successful, and if the oocyte is expressing the correct channels, or it was unsuccessful and move on to the next well. If impalement was successful, the script then checks if the voltage clamp was successful, and whether leak currents associated are within an acceptable range. If this is also successful, Roboocyte2 will then run the protocol specific portion of each script. An example of a portion of code can be seen below (Fig. 11).

```
// Impalement procedure

                Robo2.Log("Starting Oocyte Impalement...");

                Robo2.StartControlRecording();

                Robo2.Wait(2);

                ControlDisplay.SetXAxis(0, 30)
                ControlDisplay.SetYAxis_U(-60, 10)

                Robo2.Wait(5)

                if (!Impalepositive(MIN_RMP, IMPALEMENT_STEPS, IMPALEMENT_STEP, IMPALEMENT_WAIT))
                {
                    Robo2.Log("impalement failed, " + MIN_RMP + " not reached --> next oocyte");
                    Robo2.ValvePumpOff();
                    Robo2.CloseAllValves();
                    Robo2.WastePumpOff();
                        continue;
                }
        Robo2.ZMoveStepDown(50);
```

Figure 11: Sample of Roboocyte2 Scripting.
A sample of the impalement script in Roboocyte2. The script begins with the logging of impalement has begun, before impaling the oocyte. The script determines whether the impalement was successful by examining the minimum resting membrane potential of the oocyte. If the parameters were not met, the system will move on to the next well and repeat.

2.4 Shear Stress

Shear stress was modulated in the system by altering the flow speed of the peristaltic pump. To do so, the perfusion head was physically modified, and a calibration curve between shear stress applied and peristaltic pump speed was done.

2.4.1 Shear Force Perfusion Head

To assess the effects of shear force, the flow applied to each oocyte needed to be laminar. Therefore, modifications were made to the proprietary measuring head to direct a laminar flow towards the oocyte (Fig. 12). Premium Thin Wall Borosilicate glass capillary (Warner Instruments, Cat. No. 64-0784) with an outer diameter of 1.5 mm was bent, and then attached to the perfusion tube of the measuring head. The original custom perfusion head was supplied by a previous PhD student, Daniel Barth from the Department of Physiology (University of Otago) who had confirmed the flows to be laminar. Subsequent heads were hand made to mimic the original as close as possible.

Glass capillaries of the measuring electrodes were replaced after each experiment. The glass capillaries were pulled from Premium Thin Wall Borosilicate glass capillary (Warner Instruments, Cat. No. 64-0784) with an outer diameter of 1.5 mm using a flaming/brown type micropipette puller (P-87, Sutter Instruments, Novato, USA). The tips of the electrode heads needed to be 350 – 450 microns apart when in the perfusion head holder to keep the oocyte in place.

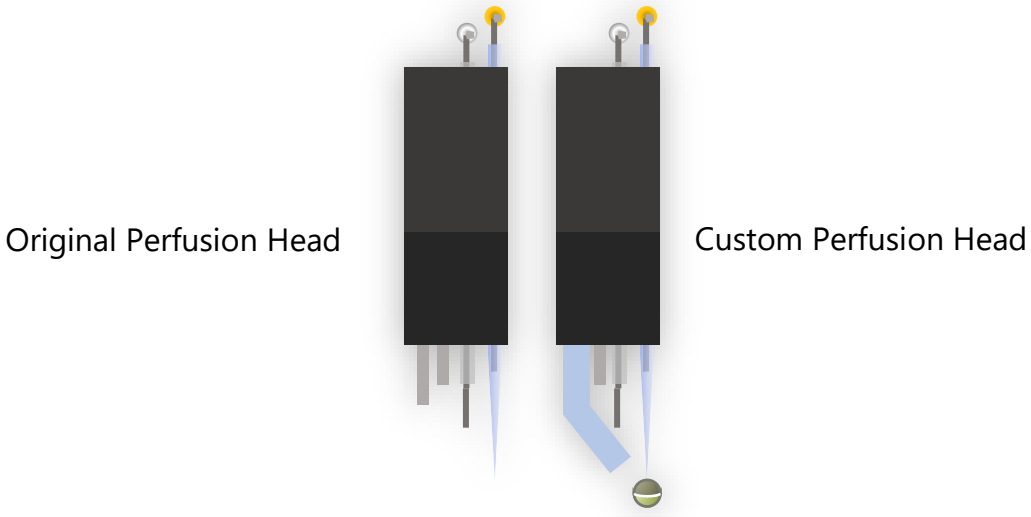

Figure 12: A comparison of the factory perfusion head and the custom perfusion head.
The proprietary perfusion head with a custom glass perfusion tube attached (right) to direct laminar shear stress to the oocyte during recording. The original perfusion head (left) would not have directed flow directly towards the oocyte.

2.4.2 Shear Force Calibration

To quantify the amount of shear stress applied to each oocyte, we first measured the flow rate of the perfusion at a range pump speeds (100-1500 au) of the peristaltic pump. We did this by measuring the mass of water collected after 5-minute perfusions at each pump speed and divided by 5 to get the mass perfused in 1 minute. Subsequently

using the mass, and the known density of water, the volume of water collected can be calculated using the equation below:

$$V = \frac{m}{\rho}$$

Equation 1: Calculation of volume
V: volume (cm^3)
m: mass (g)
ρ: density of water (g/cm^3)

This then allowed us to calculate the flow rate at each pump speed through the following equation:

$$Q = \frac{V}{t}$$

Equation 2: Calculation of flow rate
Q: flow rate (cm^3/s)
V: volume (cm^3)
t: time (s)

Following this, the flow velocity of perfusion (ω) was calculated using the following equation:

$$\omega = \frac{Q}{A}$$

Equation 3: Calculation of flow velocity
ω: flow velocity (cm/s)
Q: flow rate (cm^3/s)
A: cross-sectional area of perfusion tube (cm^3)

The Reynolds numbers (R_e) were then calculated to confirm laminar flow of perfusion using the following equation:

$$R_e = \frac{\theta \omega D}{\lambda}$$

Equation 4: Calculation of Reynolds number
R_e: Reynolds number
Θ: density of water [20 °C] (g/cm^3)
ω: flow velocity (cm/s)
D: diameter of perfusion tube (cm)
λ: kinematic viscosity of water [20 °C] (g/cm.s)

Where θ is the density of water (1 g/cm^3 at 20 °C), ω the flow velocity, D the diameter of the perfusion capillary, and λ being the kinematic viscosity of water (0.01 g/cm.s). A resulting Reynolds number below 1000 indicates laminar flow.

Following this, the effective drag force was calculated while taking into consideration of laminar flow using the equation below:

$$F_{drag} = \frac{\theta A \omega^2 C_d}{2}$$

Equation 5: Calculation of effective shear force
F_{drag}: effective drag force (dyn)
Θ: density of water [20 °C] (g/cm^3)
A: Cross sectional area of oocyte (cm^2)
ω: flow velocity (cm/s)
C_d: drag coefficient

Where F_{drag} is the effective drag force, θ is the density of water, A the cross-sectional area of an oocyte, ω the flow velocity, and C_d being the drag coefficient which has a value of 1 for R_e values in the range of 14 to 80.

Lastly, this allows us to calculate the effective shear force (F_{shear}) using the following equation:

$$F_{shear} = \frac{F_{drag}}{A}$$

Equation 6: Calculation of effective shear force
F_{shear}: shear force (dyn/cm^2)
F_{drag}: effective drag force (dyn)
A: Cross sectional area of oocyte (cm^2)

The resulting shear forces used in this experiment ranged from 0.02 to 0.236 dyn/cm^2 , and corresponds to flow rates as indicated by Figure 13 below:

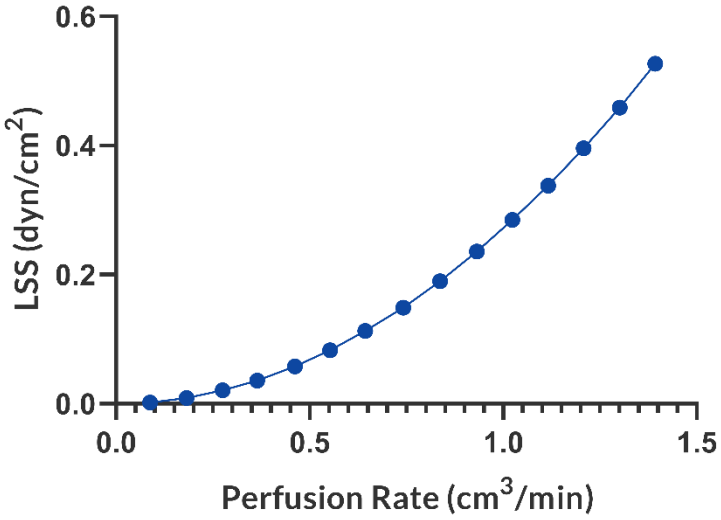

Figure 13: Calibration of Laminar Shear Stress to Perfusion Rate.
The amount of shear stress applied to the oocyte was calibrated to the perfusion rate of the peristaltic pump, ranging from 0.88 to 1.39 cm^3/min. This range produced a laminar shear stress ranging from 0 to 0.236 dyn/cm^2. This represented a range of peristaltic pump speed from 100 to 1500 au.

2.4.3 Perfusion Protocol

The perfusion protocol itself to determine the effects of shear force was finalised into the outline below:

1. Amiloride Perfusion (30 s)
2. Washout (30 s)
3. Stabilisation (90 s)
4. Step wise ORi Perfusion
   (1) 0.002 dyn/cm^2, 30 s
   (2) 0.009 dyn/cm^2, 30 s
   (3) 0.021 dyn/cm^2, 8-30 s
   (4) 0.036 dyn/cm^2, 8-30 s
   (5) 0.058 dyn/cm^2, 8-30 s
   (6) 0.083 dyn/cm^2, 8-30 s
   (7) 0.113 dyn/cm^2, 8-30 s
   (8) 0.149 dyn/cm^2, 8-30 s
   (9) 0.190 dyn/cm^2, 8-30 s
   (10) 0.236 dyn/cm^2, 8-30 s
5. Amiloride Perfusion (45 s)

Firstly, 100 µM amiloride containing ORi was applied to each well (30 s) to fully inhibit ENaC present to reduce the noise of the trace. Following this, amiloride was washed out with ORi (30 s) and perfusion was stopped to allow stabilisation of the oocyte (90 s). Then perfusion of ORi began again at a low shear stress of 0.002 dyn/cm^2 before

being increased in a 10-step wise process at set time intervals up to 0.236 dyn/cm^2 as shown in the outline above. This was done to determine whether a dose response occurs with ENaC. The time interval at step 3 and above varied between 8-30 s to account for the reduction in current seen in αβγ-ENaC. Finally, 100 μM amiloride containing ORi was perfused again to determine the amiloride sensitive current.

2.5 Carbon Monoxide

Carbon monoxide was administered to the oocyte in the form of an organic carbon monoxide releasing molecule, oCOM-21b. This is an experimental drug that was supplied by AP Ivan Sammut from the Department of Pharmacology and Toxicology (University of Otago).

2.5.1 Carbon Monoxide Perfusion system

oCOM-21b is stable in pH 6 solution and does not release Carbon Monoxide. ORi solution has a pH of 7.4 and addition of oCOM-21b to ORi results in carbon monoxide release from the molecule in a 1:1 ratio (concentration of oCOM-21b = concentration of Carbon monoxide release). Because of this, alterations to the perfusion system was necessary to minimise time between release and the perfusion well (Fig. 14).

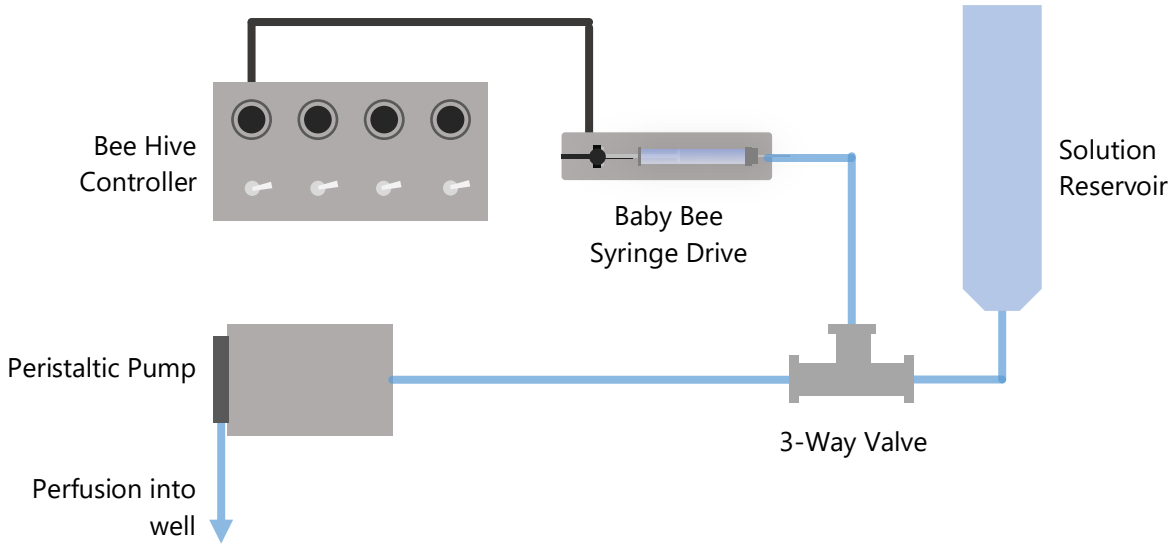

Figure 14: Schematic of carbon monoxide perfusion.
A 3-way valve was attached to the perfusion line of the peristaltic pump. This allows the attachment of a syringe containing 1 mM oCOM-21b (pH 6) to be perfused into the line. A Baby Bee Syringe Drive (Bioanalytical systems, Indiana, USA) powers the oCOM-21b perfusion, and its speed is controlled by a Bee Hive Controller (Bioanalytical systems, Indiana, USA). Depending on the speed of the Baby Bee, different concentrations of oCOM-21b may be perfused into the recording well.

Using a three-way valve, a syringe containing 1 mM oCOM-21b is connected to the perfusion system. The syringe was powered by a Baby Bee Syringe Drive (Bioanalytical systems, Indiana, USA) and controlled by a Bee Hive Controller (Bioanalytical systems, Indiana, USA). The peristaltic pump was set to 1 mL/min and by adjusting the speed of the syringe drive, different concentrations of oCOM-21b can be added to the perfusion stream. Concentrations of 0.1, 1, and 10 µM oCOM-21b was used in the perfusion by setting the speed of the syringe drive to 0.1, 1, and 10 µL/min.

2.6 Statistical Analysis

Data is expressed as the mean ± standard error of the mean (SEM). The number of experiments as *n*, while *N* indicates the number of animals from which the oocytes were harvested from. Electrophysiological data was analysed using GraphPad Prism 7. And statistical comparisons were made using one-way ANOVA analysis with multiple comparisons (column analysis), two-way ANOVA analysis with multiple comparisons (grouped analysis), and unpaired t test (comparing independent values). Tests for multiple comparisons includes Dunnett's multiple comparisons test, Sidak's multiple comparisons test and Tukey's multiple comparisons test. A p-value less than 0.05 was considered as statistically significant ($p < 0.05$ (*), $p < 0.01$ (**), $p < 0.001$ (***), $p < 0.0001$ (****)).

3

Results

3.1 The Effect of Shear stress on Human Epithelial Sodium Channels.

Here we assessed the effects of shear stress on human αβγ-ENaC and δβγ-ENaC. Shear stress was applied in a step wise manner to each oocyte from 0.002 dyn/cm^2 up to 0.236 dyn/cm^2 by altering the perfusion speed of oocyte ringer's solution (Ori). 100 μM amiloride (Ami.) perfused at the end of each recording to determine the ENaC-mediated current. The current under amiloride perfusion was subtracted from each recording to determine the amiloride sensitive current, which is the current that is due to ENaC. Then percentage activation of ENaC at each shear stress applied was calculated, with 0.24 dyn/cm^2 set as 100% activation because a plateau is seen here. Then currents at each shear stress perfused is calculated as a proportion of that 100%. From this, we then calculated the half-maximal effective shear stress for both αβγ-ENaC and δβγ-ENaC and compared these values between the two types of ENaCs.

3.1.1 Shear Stress activates αβγ-ENaC

Our results indicate that shear stress was able to activate αβγ-ENaC from 17.7 ± 1.1 % at 0.002 dyn/cm^2 up to 100 % at 0.24 dyn/cm^2 in a stepwise manner (n = 5; N = 1) (Fig. 15). And upon application of amiloride, the amiloride sensitive current was significantly reduced. This suggests a dose-dependent response of αβγ-ENaC to laminar shear stress. It is important to note that at 0.021 dyn/cm^2 and higher, the transmembrane current decreased rapidly, and the perfusion time intervals were shortened here.

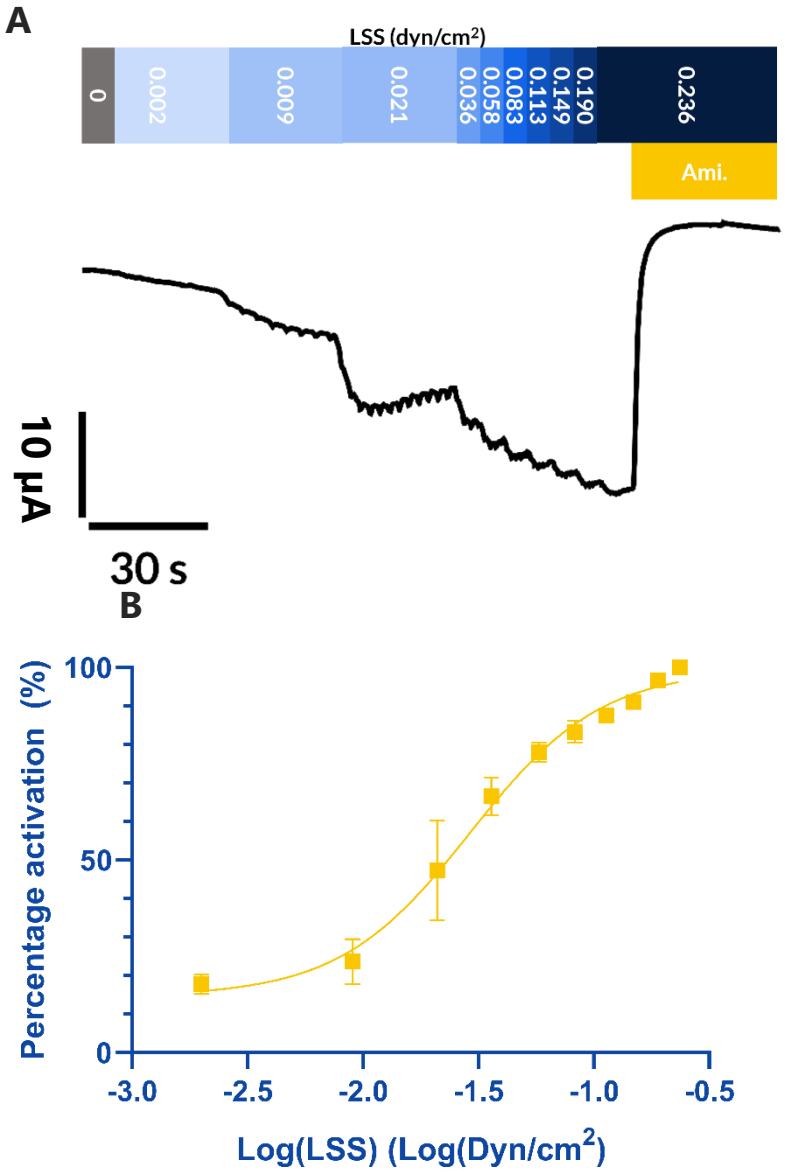

Figure 15: Shear Stress activates αβγ-ENaC.

A: Visual representative current trace of αβγ-ENaC expressing oocyte. The application of laminar shear stress (LSS) from 0.002 to 0.0236 dyn/cm^2 (blue bar) induces a stepwise increase in membrane current. The application of 100 µM amiloride (Ami., yellow bar) induces a strong decrease in membrane current and is used to determine the amiloride sensitive current. **B:** Non-Linear regression of percentage activation of αβγ-ENaC with 0.236 dyn/cm^2 set as 100 % activation. Percentage activation increased in a step wise manner as shear stress was increased in a step wise manner from 0.002 dyn/cm^2 up to 0.236 dyn/cm^2.

3.1.2 Shear stress activates δβγ-ENaC

Application of increasing amounts of shear stress showed increased in amiloride sensitive current (Fig. 16). This current was inhibited upon application of 100 µM amiloride. The results indicate that shear stress was able to activate δβγ-ENaC from 12.2 ± 2.5 % at 0.002 dyn/cm^2 up to 100 % at 0.236 dyn/cm^2 in a stepwise manner (n = 5, N = 1). Suggesting, δβγ-ENaC responds to shear stress in a dose dependent manner.

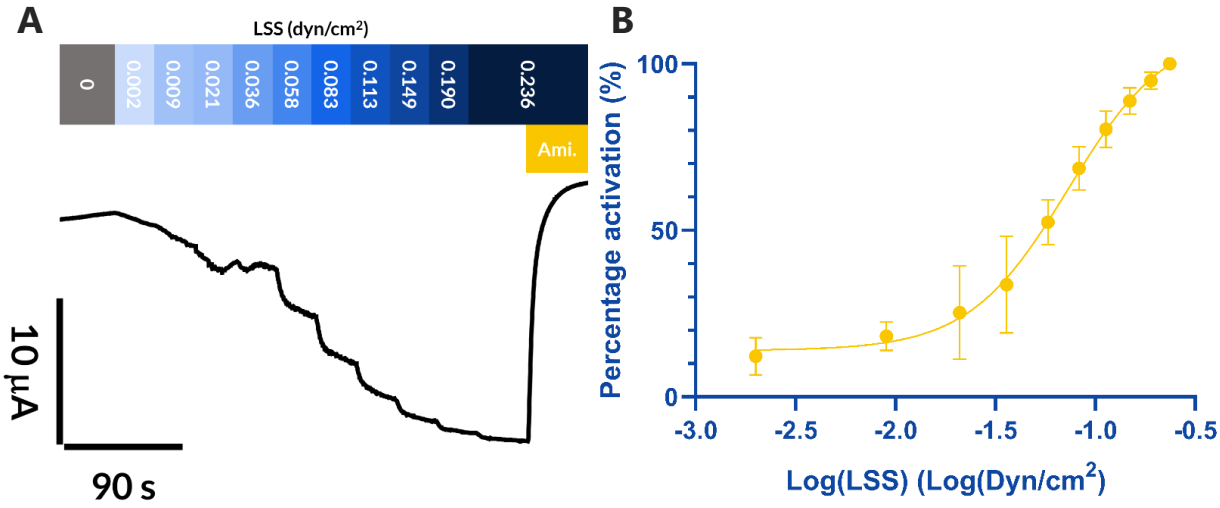

Figure 16: Human δβγ-ENaC is activated by Shear Stress.
A: Visual representative current trace of δβγ-ENaC expressing oocyte. The application of shear stress from 0.002 to 0.0236 dyn/cm^2 (blue bar) induces a stepwise increase in membrane current. The application of 100 µM amiloride (Ami., yellow bar) induces a strong decrease in membrane current and is used to determine the amiloride sensitive current. Blue arrows indicate time points where shear stress was increased **B:** Non-Linear regression of percentage activation of δβγ-ENaC with 0.236 dyn/cm^2 set as 100 % activation. Percentage activation increased in a step wise manner as shear stress was increased in a step wise manner from 0.002 dyn/cm^2 up to 0.236 dyn/cm^2.

3.1.3 δβγ-ENaC is more sensitive to shear stress than αβγ-ENaC

From Figures 15B and 16B, the half-maximal effective shear stress for both αβγ-ENaC and δβγ-ENaC can be determined. δβγ-ENaC had a statistically higher EC_{50} of 0.069±

0.007 dyn/cm^2 when compared to αβγ-ENaC, which had an EC_{50} of 0.029± 0.003 dyn/cm^2 (n = 5, N = 1, ***: p = 0.001). This suggests αβγ-ENaC is more sensitive to shear stress than δβγ-ENaC. Meaning, for the same amount of shear stress, αβγ-ENaC would provide a higher transmembrane current when compared to δβγ-ENaC.

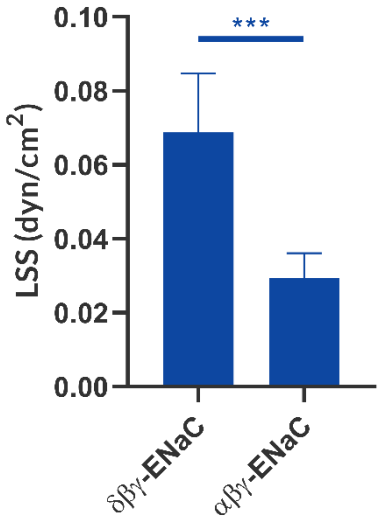

Figure 17: Comparison of half-maximal effective shear stress (EC_{50}) between αβγ-ENaC and δβγ-ENaC.
The EC_{50} of αβγ-ENaC and δβγ-ENaC was compared. δβγ-ENaC (n=5) had a significantly higher EC_{50} when compared to αβγ-ENaC (n=5). Unpaired t-test; ***: p < 0.001.

3.1.4 Shear stress effect in *Xenopus* oocytes due to ENaC activation.

It can be confirmed that the effects observed via shear stress application was due to ENaC activation. This can be seen in the water injected control oocytes, where no ENaC was expressed (Fig. 18). Application of shear stress in water injected oocytes resulted in no change in current when shear stress or amiloride was applied.

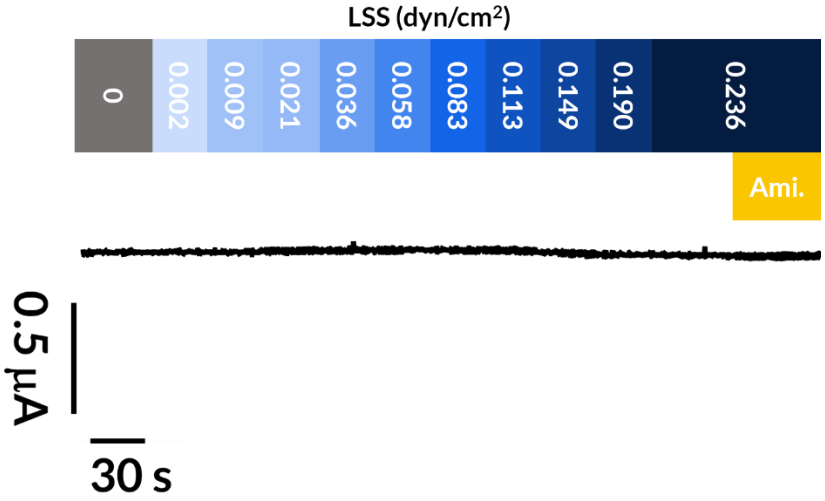

Figure 18: Control experiment for shear stress application.
Representative current trace of shear stress application on water-injected oocytes. No effect can be seen with shear stress application, nor was an effect seen under amiloride perfusion.

3.2 The effect of carbon monoxide on human epithelial sodium channels

oCOM-21b, an organic carbon monoxide releasing molecule was used to assess the effect of carbon monoxide on human αβγ-ENaC and δβγ-ENaC. oCOM-21b was perfused at concentrations of 0.1, 1.0, and 10 μM to determine its effect on ENaC expressed on *Xenopus* oocytes. The flow was constant throughout the procedure to minimize shear stress effects. A time control was also performed where only Ori, without oCOM-21b was perfused over the same length of perfusion time to control for run-down currents. Then the time course of the effect at 2 minutes intervals over a 6-minute perfusion of each concentration was plotted in αβγ-ENaC and δβγ-ENaC.

However, due to the complexity of the carbon monoxide response as no significant result was observed, the data is further analyzed in other ways. The ratio of amiloride sensitive current at 6 minutes (t_6) over the transmembrane current at 0 minutes (t_0) oCOM-21b perfusion were calculated at each concentration to get a measure of proportionate change in amiloride sensitive current. A t_6/t_0 ratio below 1 would indicate a decrease in amiloride sensitive current over the course of the perfusion, whereas a ratio over 1 indicates an increase in amiloride sensitive current, and a ratio of 1 indicates no change in amiloride sensitive current.

Furthermore, a linear regression was done for the 6-minute perfusions to determine the slope of the traces. This tells us the rate of change in amiloride sensitive current. These were then compared against the time control to determine if there was a

difference in rate of change between the concentrations of oCOM-21b as well as between αβγ-ENaC and δβγ-ENaC.

3.2.1 Carbon Monoxide effect on αβγ-ENaC

Oocyte was perfused initially with Ori to washout the initial amiloride perfused, followed by oCOM-21b at the same perfusion rate to minimize effect of shear stress. Amiloride (100 μM) was perfused at the end of each recording to determine the ENaC-mediated current. A time control was done where no oCOM-21b was perfused over the same length of time to compare for effects of run-down currents in the oocyte. All treatments showed an increase in current during the wash off of amiloride, and the current gradually decreased over the course of the oCOM-21b perfusion. And a sharp decrease in current was seen upon amiloride application at the end (Fig. 19).

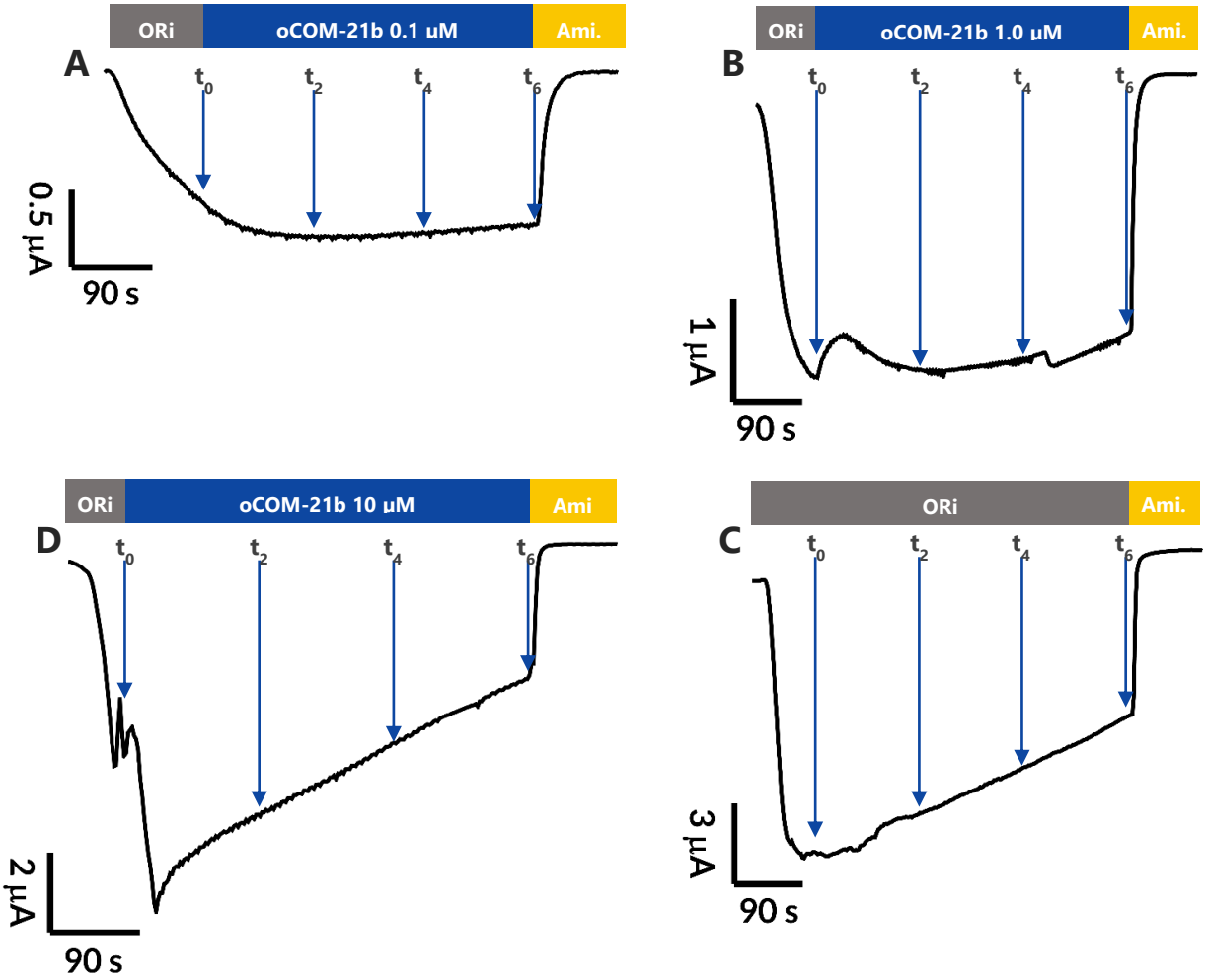

Figure 19: Representative current traces of αβγ-ENaC expressing oocytes.
A, B, C) Representative current trace of αβγ-ENaC expressing oocytes being perfused with oCOM-21b at 0.1, 1.0, and 10 µM concentrations respectively. 100 µM amiloride (Ami.) perfusion at the end resulted in a strong decrease in current and is used to determine the amiloride sensitive current. **D)** Representative current trace of αβγ-ENaC expressing oocytes being perfused with Ori as a time control (TC) for the experiment.

Quantitively, statistical differences were found at t_0 between the time control (-5.4 ± 1.6 µA, n = 4) and 0.1 (-1.1 ± 0.5 µA, n = 4, **: $p < 0.01$), 1.0 (-2.4 ± 0.6 µA, n = 5, *: $p < 0.05$), and 10 (-8.6 ± 0.3 µA, n = 3, *: $p < 0.05$) µM oCOM-21b (Fig. 20). Because all oocytes have undergone the same treatment by t_0, they should theoretically be very similar to each other with similar currents. But because they were all statistically different from the time control, it is likely there is high variability between each oocyte.

At t_2, a significant difference was found between the time control (-4.8 ± 1.5 µA, n = 4) and 0.1 µM oCOM-21b (-1.48 ± 0.35 µA, n = 4, *: $p < 0.05$). No other significant differences were found between the time control and oCOM-21b treatments over the 6 minute perfusion period. Statistical differences found at t_0 suggests large variability in αβγ-ENaC expressing oocytes as treatment until then had been identical between all groups.

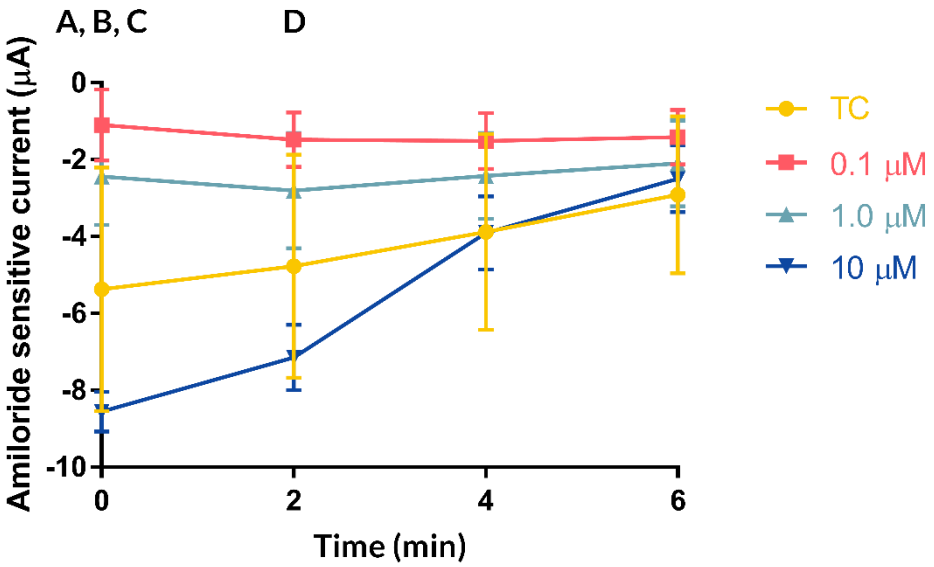

Figure 20: Effect of carbon monoxide on αβγ-ENaC expressing oocytes.
At t0, all concentrations of oCOM-21b perfusion were significantly different when compared to the time control (TC). At t2, only 0.1 µM oCOM-21b perfusion was significantly lower when compared to the time control. No other statistically significant differences were found between oCOM-21b perfusion and the time control at any concentration or time point. 2way ANOVA, Dunnett's multiple comparisons test; **A**: at t0 between TC and 0.1 µM, $p < 0.001$; **B**: at t0 between TC and 1.0 µM, $p < 0.05$; **C**: at t0 between TC and 10 µM, $p < 0.05$; **D**: at t2 between TC and 0.1 µM, $p < 0.05$.

Examining the t_6/t_0 ratio of each concentration (Fig. 21), no significant differences were found between the time control (0.5 ± 0.2, n = 4) and 0.1 (2.1 ± 1.0, n = 4), 1.0 (1.0 ± 0.2, n = 5), and 10 (0.3 ± 0.1, n = 3) µM oCOM-21b perfusions ($p = 0.14$). But a biphasic

trend could be seen as at a low concentration of oCOM-21b (0.1 µM), the mean t_6/t_0 ratio was above one suggesting a stimulatory response. But at a higher concentraion, the ratio was below 1, suggesting an inhibitory response. This suggests a possible concentration dependent effect of oCOM-21b.

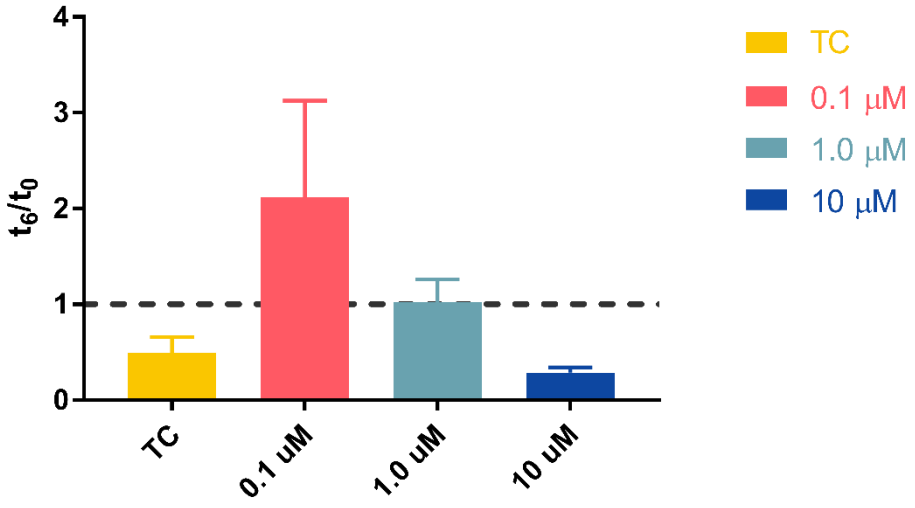

Figure 21: t_6/t_0 ratios in αβγ-ENaC expressing oocytes.
No statistical significances were found between the time control t_0/t_6 ratio and any of the oCOM-21b perfusion concentrations. One-way ANOVA, Tukey's multiple comparisons test.

Examining the slope of each treatment (Fig. 22), significant differences are found between the time control (0.41 ± 0.03 µA/min, n = 4) and 0.1 (-0.05 ± 0.04 µA/min, n = 4, p = 0.002), 1.0 (0.07 ± 0.06 µA/min, n = 5, p = 0.010), 10 (1.07 ± 0.13 µA/min, n = 3, p = 0.001) µM. Furthermore, the slope at 10 µM oCOM-21b perfusion was significantly greater compared to both 1.0 µM ($p < 0.0001$) and 0.1 µM ($p< 0.0001$) oCOM-21b perfusion. Suggesting, at 10 µM oCOM-21b perfusion, the rate of decrease in current is significantly increased compared to the lower perfusion concentrations. This further supports the idea of the biphasic trend noted earlier. It is important to note

here that a positive slope is a reduction in current as the amiloride sensitive currents are negative values.

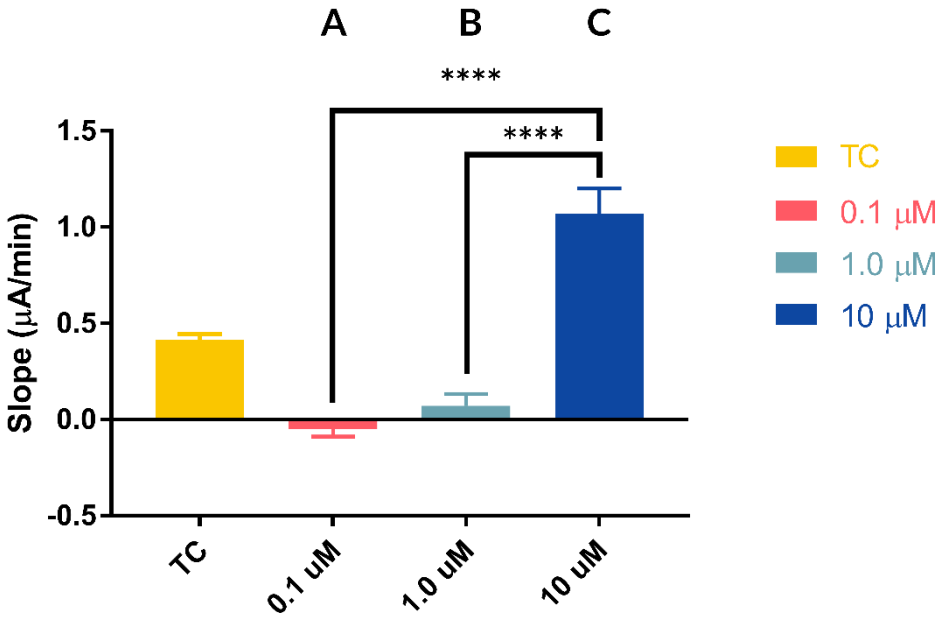

Figure 22: Slopes of αβγ-ENaC expressing oocytes.
Slopes of each treatment was obtained using linear regression, and slopes of all oCOM-21b perfusions were significantly different when compared to the time control. 10 µM oCOM-21b perfusion had a significantly steeper slope when compared to 1.0 and 0.1 µM oCOm-21b perfusions. Ordinary one-way ANOVA, Tukey's multiple comparisons test; **A**: between TC and 0.1 µM, $p < 0.001$; **B**: between TC and 1.0 µM, $p < 0.001$; **C**: between TC and 10 µM, $p < 0.0001$; ****: $p < 0.00001$.

In summary, these results suggest carbon monoxide released by oCOM-21b causes some effects in αβγ-ENaC expressed on *Xenopus* oocytes involving a biphasic response. But no statistically significant evidence for the effect of carbon monoxide on αβγ-ENaC was found.

3.2.2 Effect of Carbon Monoxide on δβγ-ENaC

The exact same protocol done on αβγ-ENaC expressing oocytes was repeated on δβγ-ENaC expressing oocytes. And again, visually, the recordings for each treatment were similar with an increase in current seen during the wash off of amiloride. The current then decreased gradually over the course of the perfusion time and was significantly reduced upon amiloride administration. A large discrepancy in the scale bar is noted and suggests a high variation in the number of ENaC expressed on the surface between each oocyte (Fig. 23).

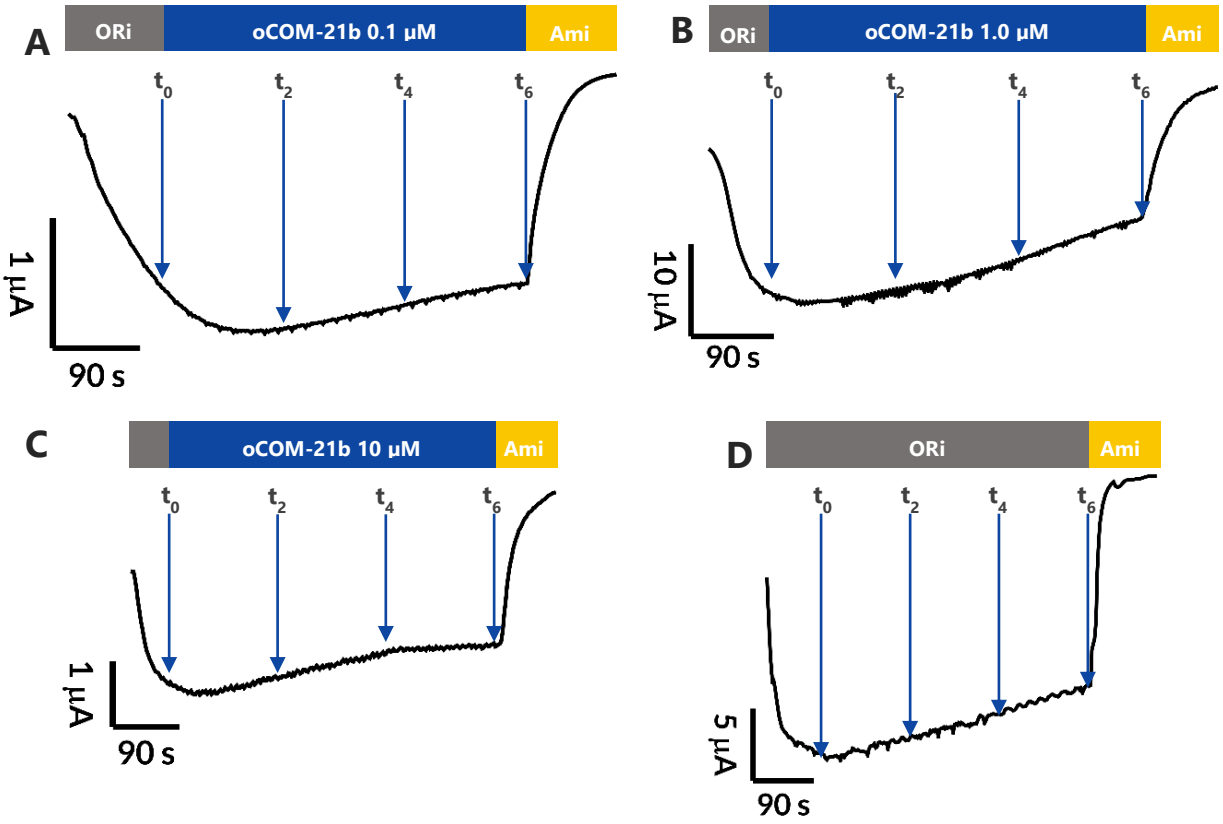

Figure 23: Representative current traces of δβγ-ENaC expressing oocytes.
A, B, C) Representative current trace of δβγ-ENaC expressing oocytes being perfused with oCOM-21b at 0.1, 1.0, and 10 µM concentrations respectively. 100 µM amiloride (Ami.) perfusion at the end resulted in a strong decrease in current and is used to determine the amiloride sensitive current. **D)** Representative current trace of δβγ-ENaC expressing oocytes being perfused with Ori as a time control (TC) for the experiment.

Quantitively, no statistical differences were found between the time control and any concentrations of oCOM-21b perfused at any time point in δβγ-ENaC expressing *Xenopus* oocytes (Fig. 24). This suggests that there is oCOM-21b likely has no effect on δβγ-ENaC.

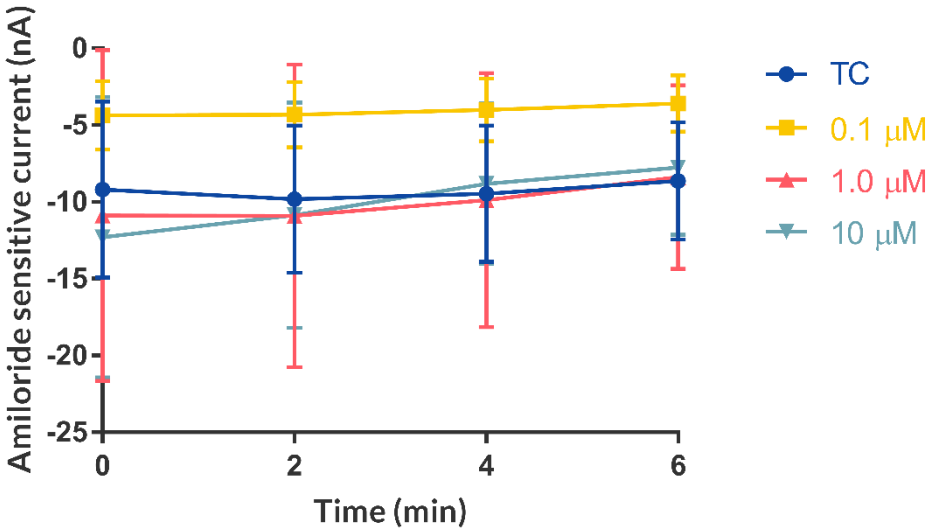

Figure 24: Effect of carbon monoxide on δβγ-ENaC expressing oocytes.
No significant differences were found between the time control and any oCOM-21b concentration at any time point. 2way ANOVA, Dunnett's multiple comparisons test.

Furthermore, examining the t_6/t_0 ratios (Fig. 25), no statistical differences were found between the time control and all concentrations of oCOM-21b perfused at any time point in δβγ-ENaC expressing Xenopus oocytes. This further suggests that carbon monoxide may have no effect on δβγ-ENaC.

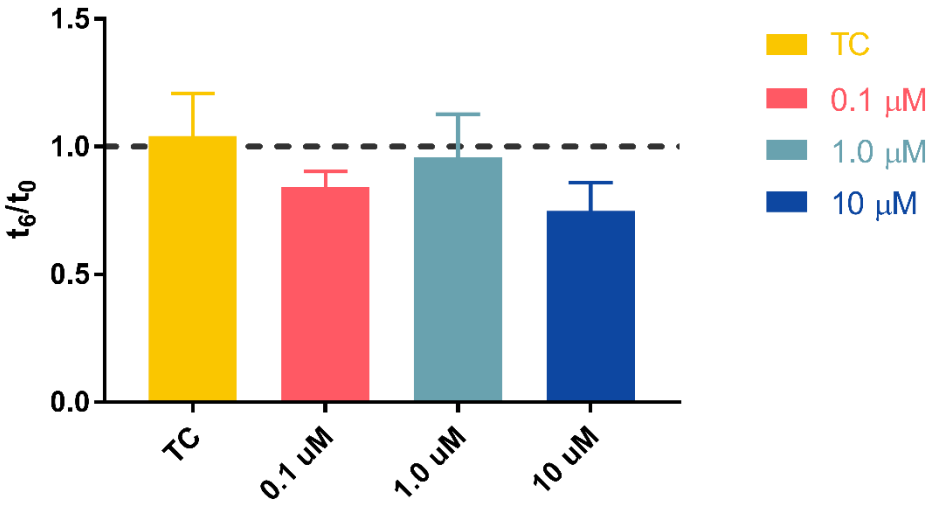

Figure 25: t_6/t_0 response to carbon monoxide in δβγ-ENaC.
No statistical significances were found between the time control t_0/t_6 ratio and any of the oCOM-21b perfusion concentrations. Ordinary one-way ANOVA, Dunnett's multiple comparisons test.

Examining the slope of each recording (Fig. 26), only 10 µM (0.75 ± 0.06 µM/min, n = 5) oCOM-21b treatment was statistically higher when compared to the time control (0.10 ± 0.12 µM/min, n = 5) ($p < 0.004$). No statistical differences were found between the time control and 0.1 µM (0.13 ± 0.03, n = 4, p = 0.99), as well as 1.0 µM (0.42 ± 0.12, n = 3, p = 0.14). A trend can be observed where a higher concentration of oCOM-21b results in a greater slope. This suggests at higher concentrations of oCOM-21b, a greater rate of decrease in amiloride sensitive current may be observed in δβγ-ENaC. Again, it is important to note that a slope above 0 is an inhibitory response as the amiloride sensitive current values were negative when measured.

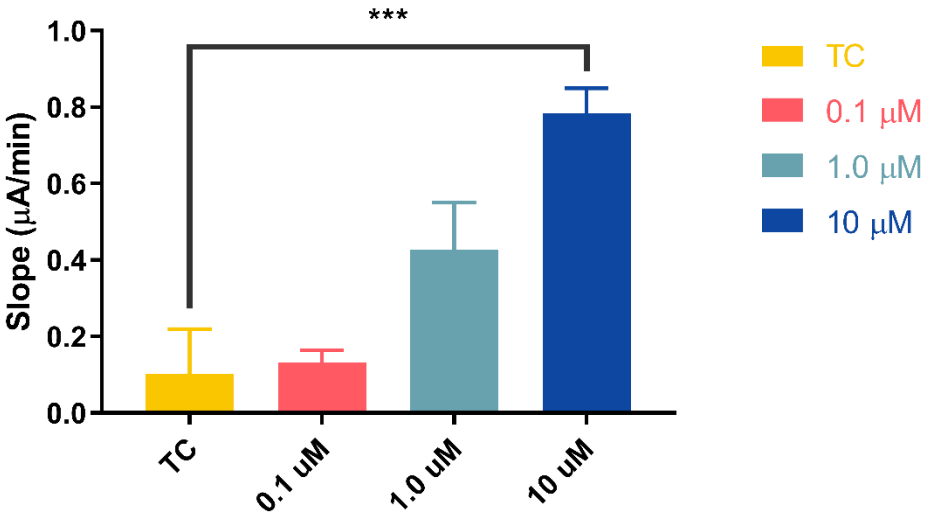

Figure 26: Slopes of δβγ-ENaC expressing oocytes.
Slopes of each treatment was obtained using linear regression, no statistical significance were found between any group. Ordinary one-way ANOVA, Tukey's multiple comparisons test.

These results suggest δβγ-ENaC is not affected by carbon monoxide released by oCOM-21b at any concentration. However, this is likely due to the limited number of experiments performed as some trends are still visible such as in Figure 26 where there is a general increase in slope as the concentration of oCOM-21b was increased.

3.2.3 The effect of carbon monoxide compared between αβγ-ENaC and δβγ-ENaC.

The t_6/t_0 ratios (Fig. 27) were compared between αβγ-ENaC expressing oocytes and δβγ-ENaC expressing oocytes. We found that there were no significant differences between the two types of ENaCs at any concentration of oCOM-21b. This suggests that the response is similar between the two ENaCs but it must be noted that the biphasic trend observed in αβγ-ENaC response to carbon monoxide was not found in δβγ-ENaC.

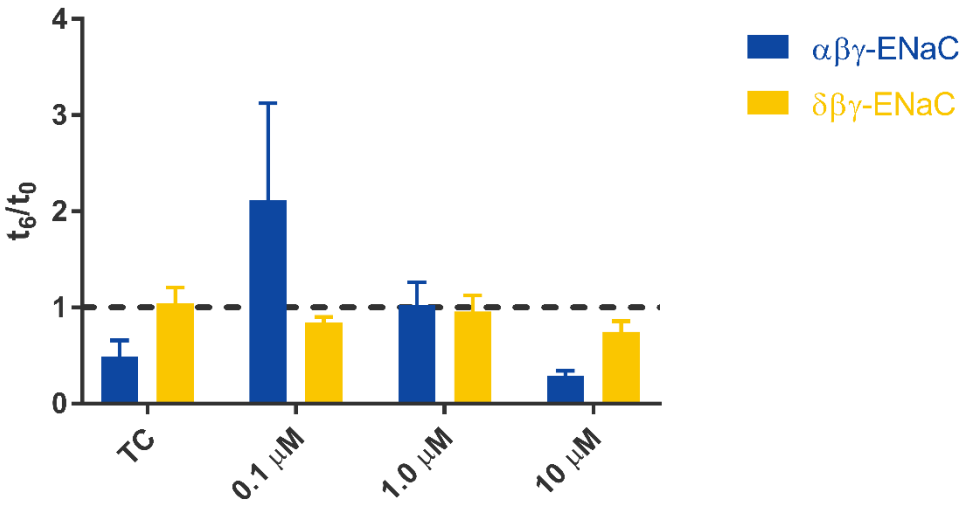

Figure 27: Comparison of t_6/t_0 ratios between αβγ-ENaC and δβγ-ENaC.
No statistical significance was found in any treatment between αβγ-ENaC and δβγ-ENaC. 2way ANOVA, Sidak's multiple comparisons test

However, when comparing the slopes of each treatment between αβγ-ENaC expressing oocytes and δβγ-ENaC expressing oocytes (Fig. 28), we found that the time control of αβγ-ENaC (0.41 ± 0.03 μA/min, n = 4) had a significantly higher slope when compared to δβγ-ENaC (0.10 ± 0.12 μA/min, n = 5, p = 0.036). And at 1.0 μM oCOM-21b perfusion, δβγ-ENaC (0.42 ± 0.12 μA/min, n = 3) had a significantly higher slope when compared to αβγ-ENaC (0.07 ± 0.06 μA/min, n = 5, p = 0.026)). This suggests variation in response between the two ENaCs to carbon monoxide does exist.

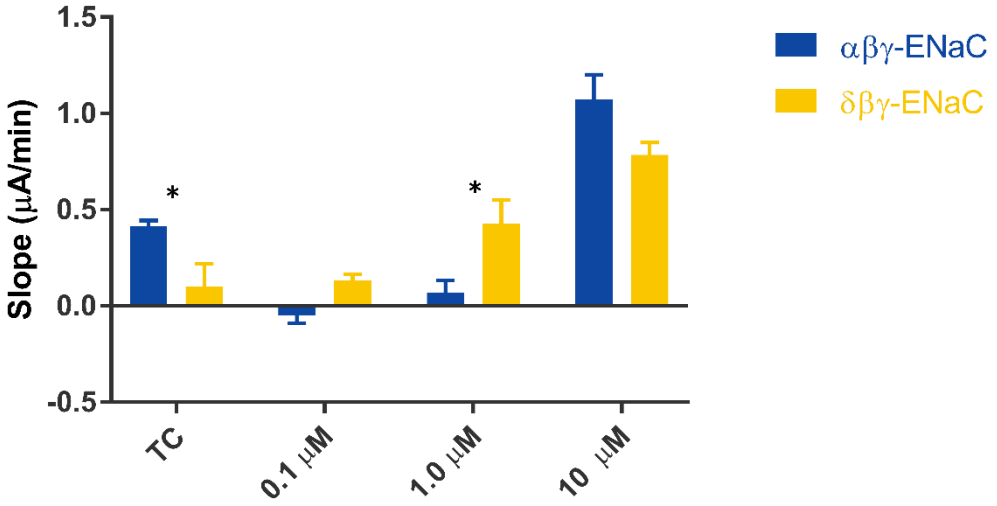

Figure 28: Comparison of slopes between αβγ-ENaC and δβγ-ENaC.
The time control (TC) of αβγ-ENaC had a significantly steeper slope when compared to δβγ-ENaC. And at 1.0 μM oCOM-21b perfusion, δβγ-ENaC is significantly steeper compared to αβγ-ENaC. 2way ANOVA, Sidak's multiple comparisons test; *: $p < 0.05$.

4

Discussion

4.1 Overview

Hypertension, where blood pressure is increased, results in increased shear stress. We aimed to determine how this increase in shear stress may affect αβγ-ENaC and δβγ-ENaC mediated sodium transport using TEVC. We hypothesized αβγ-ENaC and δβγ-ENaC both respond to shear stress in a dose dependent manner, and the response is likely to be similar between the two types of ENaCs. From our results we were able to confirm both forms of ENaC are responsive to shear stress, however, αβγ-ENaC was more sensitive to shear stress. Furthermore, increased ENaC activity in the arterial endothelium has been shown to inhibit vascular relaxation (Perez *et al.*, 2009), potentially exacerbating the effects of hypertension.

Carbon monoxide have been shown in previous studies to be an inhibitor of αβγ-ENaC activity (Althaus *et al.*, 2009), making it a potential treatment in hypertension. But unpublished data from the Fronius lab has also found δβγ-ENaC to be present in arteries, and how carbon monoxide affects δβγ-ENaC is unknown. Therefore, we aimed to examine whether carbon monoxide could potentially inhibit δβγ-ENaC mediated sodium transport, and how the effect compares to αβγ-ENaCs. Doing so would pave way in placing carbon monoxide as a potential therapeutic in the treatment of hypertension. We hypothesized carbon monoxide would inhibit ENaC mediated sodium transport in both αβγ-ENaC and δβγ-ENaC. But instead, we found that carbon monoxide applied in the form of an organic carbon monoxide releasing molecule, oCOM-21b had no effect on ENaC mediated sodium transport in both ENaCs.

4.2 ENaC is activated by shear stress

Shear stress is the stress applied to the walls of an object by the frictional forces of a passing flow of fluid. In humans, this phenomenon is found in many regions, but importantly in regard to hypertension, shear stress is found in the vasculature. In the vasculature, blood flow exerts frictional forces against the surrounding endothelium. And under hypertension, where blood flow is increased, the shear stress applied to the surrounding endothelium is also increased.

This is relevant to ENaC as ENaC has been shown to be mechanosensitive and responsive to shear stress (Carattino *et al*., 2004; Althaus *et al*., 2007; Fronius *et al*., 2010; Abi-Antoun *et al*., 2011). Shear stress has been shown to upregulate ENaCs open probability (Fronius *et al*., 2010), allowing greater Na+ transport. And increased ENaC-mediated sodium transport has been shown to inhibit vascular relaxation via inhibition of eNOS (Perez *et al*., 2009). This is particularly relevant in hypertension where shear stress is elevated, which would stimulate ENaC activity, resulting in inhibited vascular relaxation, which potentially exacerbates hypertension. Furthermore, unpublished data from the Fronius lab has found δβγ-ENaC to be present in human arteries. Therefore, understanding how δβγ-ENaC responds to shear stress in comparison to αβγ-ENaC may allow further insights into hypertension, and the development of new potential therapeutics in its treatment.

4.2.1 ENaC responds to shear stress in a dose dependent manner.

Our results confirm both human αβγ-ENaC and δβγ-ENaC expressed on Xenopus oocytes respond to shear stress in a dose-dependent manner. The αβγ-ENaC response is consistent with previous literature done using ENaC from multiple species including mouse (Satlin *et al*., 2001; Carattino *et al*., 2004; Karpushev *et al*., 2010), Xenopus laevis (Althaus *et al*., 2007), and humans (Fronius *et al*., 2010). δβγ-ENaCs response to shear stress is also consistent with previous literature as shown in a study also done using Xenopus laevis oocytes (Abi-Antoun *et al*., 2011). However, this is the first evidence to confirm a dose-dependent response in δβγ-ENaC to shear stress. This is important as it suggests depending on the severity of hypertension, δβγ-ENaC may produce a different amount of ENaC-mediated sodium transport. But it is unclear whether δβγ-ENaC may influence eNOS activity.

The mechanism behind the αβγ-ENaC inhibition of eNOS is currently unclear, other than knowing it involves the PI3K/Akt pathway (Perez *et al*., 2009). However, given increased shear stress on αβγ-ENaC and δβγ-ENaC both result in an increased inwards sodium current, it is likely that δβγ-ENaC would also produce an inhibitory effect on eNOS. Furthermore, since the data also suggests αβγ-ENaC is more sensitive to shear stress than δβγ-ENaC, meaning changes in shear stress would produce a greater change in response in αβγ-ENaC. It is likely that αβγ-ENaC would affect eNOS to a greater degree than δβγ-ENaC under the same amount of shear stress. Therefore, if the mechanism of interaction between ENaC and eNOS is dependent on abundance of sodium ions, αβγ-ENaC would produce a greater effect.

However, it is important to know that much of this is still speculation as the mechanism is still not confirmed. And furthermore, one study has indicated that there is no interaction between ENaC and eNOS (Ydegaard *et al*., 2019), but they were also unable to consistently identify the presence of ENaC in the arteries and endothelium, which confounds their result. Therefore, it is important further confirm the exact mechanism in order to have a full grasp of the influence of ENaC on eNOS.

4.3 Carbon Monoxide and ENaC

Carbon monoxide administered in the form of carbon monoxide releasing molecules (CORMS) is under research as a potential treatment of cardiovascular diseases (Kim & Choi, 2018). CORMs have also been shown to influence αβγ-ENaC, but the effect on δβγ-ENaC is unknown. However, given it is now known that ENaC-mediated sodium transport by both ENaCs is upregulated under increased shear stress such as during hypertension. It would be advantageous in confirming whether carbon monoxide is a potential inhibitor of ENaC as a potential therapeutic in the treatment of hypertension.

4.3.1 Carbon monoxide may have a concentration dependent effect on αβγ-ENaC

At the outset, no statistically significant result was seen upon the application of carbon monoxide on αβγ-ENaC at all concentrations perfused when compared to the time control. This would contradict against current literature as it has been shown carbon monoxide influences αβγ-ENaC activity. However, upon further analysis of the data, a biphasic trend was noted through the t6/t0 ratios and the rate of change in amiloride

sensitive current. This provides potential insights into the conflicting literature on the effect of carbon monoxide on αβγ-ENaC now.

Current literature on the effect of carbon monoxide on αβγ-ENaC suggests both inhibitory (Althaus *et al*., 2009) and stimulatory (Wang *et al*., 2009) effects. And it is currently suggested this is a tissue specific response (Wilkinson & Kemp, 2011) as the two studies were done in different type of tissues, one in lung tissue of rabbits, whilst the other was done in kidney tissue of mice. However, one other notable difference between the two studies besides the type of tissue was the amount of carbon monoxide perfused. The study with the inhibitory response perfused the tissue with 100 μM of carbon monoxide donor (Althaus *et al*., 2009), whereas the stimulatory response was perfused with 100 nM of carbon monoxide donor (Wang *et al*., 2009). This reflects the biphasic trend observed in this project, suggesting ENaC can respond differently depending on the concentration of carbon monoxide perfused.

This is not the first known case of a biphasic response in ENaC. ENaC has also been shown to have a biphasic response to other stimulants including gadolinium (Knoepp *et al*., 2017). It was shown that a low concentration of gadolinium resulted in upregulation of ENaC activity, whilst high concentration of gadolinium resulted in reduced ENaC activity. The authors here proposed that ENaC had multiple binding sites for gadolinium that are concentration specific. Whether this mechanism is similar regarding carbon monoxide is unclear, however, Wang *et al* (2009) did show that the inhibitory response was likely due to direct interaction between carbon monoxide and histidine residues of αβγ-ENaC. As multiple histidine residues have been shown to be

able to modulate αβγ-ENaC mediated sodium transport (Sheng *et al.*, 2004), it does suggest the theory of multiple binding sites for carbon monoxide in αβγ-ENaCs is plausible. Further research to confirm the binding sites would place a clearer understanding in the mechanism behind the biphasic response.

4.3.2 Carbon monoxide had no effect on δβγ-ENaC

This project also showed no statistically significant changes in δβγ-ENaC-mediated sodium transport upon application of carbon monoxide at any concentration when compared to the time control. And furthermore, the biphasic response trend was not observed. Instead, it was noted that there was a dose dependent trend when examining the rate of change of amiloride sensitive current. It was shown that increased amount of carbon monoxide lead to increased rate of decrease in amiloride sensitive current. This suggests carbon monoxide likely causes an inhibitory effect on δβγ-ENaC.

However, as no other studies has examined the effect of carbon monoxide on δβγ-ENaC, it is difficult to elucidate further information. But, if further studies confirm an inhibitory effect on δβγ-ENaC, the inhibitory effect could be advantageous in the treatment of hypertension, by reducing eNOS inhibition.

The reasoning for the lack of significance in the results here likely arises from the severely limited number of experiments, with no more than 5 oocytes tested for each concentration of carbon monoxide all coming from a single frog. This combined with the high variability that was noted at time 0 makes it difficult to determine significance. This variability in ENaC injected oocytes is further supported by a previous PhD project (Barth D, 2017). Therefore, it would be of significant benefit in repeating the experiment

using greater number of oocytes, from different frogs. Doing so would provide a more definite answer on the effect of carbon monoxide on δβγ-ENaC.

4.3.3 Comparing the effect of carbon monoxide between αβγ-ENaC and δβγ-ENaC

Because the α subunit and δ subunit only share 34% gene identity (Hanukoglu & Hanukoglu, 2016), it is expected that they function differently when exposed to carbon monoxide. This is noted as the biphasic trend was only observed in αβγ-ENaC and not in δβγ-ENaC. And furthermore, statistically significant difference in rate of change in current between the two ENaCs was found at 0.1 μM carbon monoxide perfusion. This suggests the binding site that is responsible for the low carbon monoxide concentration induced stimulation of αβγ-ENaC is likely dependent on the α subunit.

However, with the limited data available from this project, and current literature on the effect of carbon monoxide on αβγ-ENaC, it is difficult to further interpret these findings.

4.4. Methodological considerations and future directions

Although it was to the best of our abilities to consider factors that may influence the outcome of our results, some factors were unable to be controlled for due to the nature of the project.

1. We are unable to confirm that the shear stress applied to the oocyte was laminar due to the shape of the well. This is because the perfusion well is not set up in a linear fashion, where there is a net flow from one direction to the other. Instead, the current is U shaped, and may result in turbulent flow that exerts an uncertain and unprecise

amount of shear stress on ENaC. However, a dose response was still found suggesting that the turbulent flow may not have a detrimental effect on the experiment.

2. The amount of shear stress applied in this project may not reflect that actual amount of shear stress experienced by the endothelium in arteries. It has been shown shear stress in arteries may rise to ~ 70 dyn/cm2 (Lipowsky, 1995), which is significantly higher than the 0.236 dyn/cm2 tested here. However, it is important to note that although the lumen of the artery could reach the 70 dyn/cm2 value, the actual surface of the endothelium may experience significantly reduced amount of shear stress .This is due to the glycocalyx of the endothelium, which may provide a shielding effect on the surface itself, significantly reducing the amount of shear stress experienced on the surface of the endothelium (van den Berg *et al.*, 2006). Therefore, it would be beneficial in devising a method in determining the actual amount of shear stress experienced by the endothelial cell surface itself.

3. Our results cannot be directly translated to the human system. Oocytes and the human endothelium are structurally different and may therefore affect the interaction between ENaC and Shear Stress. Therefore, further experimentation should be done where ENaC is expressed in human cell lines such as HUVEC to confirm the findings in this project.

4. There seems to be a large variability in ENaC expression in oocytes. This is seen most clearly in Figure 20 as at time 0, all treatment groups were statistically different to the time control even though they had undergone the exact same procedure up to

that point. Therefore, it is important in ensuring a larger sample size of oocytes from different frogs to account for this variability.

5. We were unable to confirm the successful release of carbon monoxide from oCOM-21b. Although we know that oCOM-21b releases carbon monoxide at pH 7.4, the pH of the Ori perfusion solution, we are unable to confirm if CO was able to be released during the perfusion time. Furthermore, due to the gaseous nature of carbon monoxide, we were unable to confirm the actual concentration of the gas present in the well during recording.

4.5 Conclusion and future directions

In conclusion, increased shear stress under hypertension can upregulate ENaC-mediated sodium transport in both types of ENaCs. This confirms the initial hypothesis was correct. However, given the exact mechanism behind the interaction between ENaC and eNOS is unclear, we are unable to confirm the effect on hypertension itself. Furthermore, carbon monoxide was not found to statistically significantly affect either forms of ENaC. But trends were observed, and further experimentation should be done to confirm these trends.

Based on our results, a few different directions for investigation are open. As the current literature on the effect of carbon monoxide on ENaC remains elusive, confirming the biphasic trend observed in αβγ-ENaC in response to carbon monoxide would aid in the development of carbon monoxide in the treatment of hypertension. Additionally, patch clamp experimentation would be beneficial here as it would allow detailed and nuanced investigation into the underlying mechanism. The role of δβγ-ENaC in hypertension is still unclear, therefore, confirming whether δβγ-ENaC may also inhibit vascular relaxation through the same eNOS pathway as αβγ-ENaC would provide insight into δβγ-ENaCs role in hypertension.

References

Abeyrathna N, Washington K, Bashur C & Liao Y. (2017). Nonmetallic carbon monoxide releasing molecules (CORMs). *Organic & Biomolecular Chemistry* **15,** 8692-8699.

Abi-Antoun T, Shi S, Tolino LA, Kleyman TR & Carattino MD. (2011). Second transmembrane domain modulates epithelial sodium channel gating in response to shear stress. *American journal of physiology Renal physiology* **300,** F1089-F1095.

Althaus M, Bogdan R, Clauss WG & Fronius M. (2007). Mechano-sensitivity of epithelial sodium channels (ENaCs): laminar shear stress increases ion channel open probability. *The FASEB Journal* **21,** 2389-2399.

Althaus M, Fronius M, Buchackert Y, Vadasz I, Clauss WG, Seeger W, Motterlini R & Morty RE. (2009). Carbon monoxide rapidly impairs alveolar fluid clearance by inhibiting epithelial sodium channels. *American Journal of Respiratory Cell and Molecular Biology* **41,** 639-650.

Barth D. (2017). Characterising the effect of shear force on the activity of the epithelial sodium and acid sensing ion channels (PhD). University of Otago.

Bollag WB. (2011). Regulation of aldosterone synthesis and secretion. *Comprehensive Physiology* **4,** 1017-1055.

Bolotina VM, Najibi S, Palacino JJ, Pagano PJ & Cohen RA. (1994). Nitric oxide directly activates calcium-dependent potassium channels in vascular smooth muscle. *Nature* **368,** 850-853.

Brune B & Ullrich V. (1987). Inhibition of platelet aggregation by carbon monoxide is mediated by activation of guanylate cyclase. *Molecular Pharmacology* **32,** 497-504.

Canessa CM, Horisberger J-D & Rossier BC. (1993). Epithelial sodium channel related to proteins involved in neurodegeneration. *Nature* **361,** 467.

Canessa CM, Schild L, Buell G, Thorens B, Gautschi I, Horisberger J-D & Rossier BC. (1994). Amiloride-sensitive epithelial Na+ channel is made of three homologous subunits. *Nature* **367,** 463.

Carattino MD, Liu W, Hill WG, Satlin LM & Kleyman TR. (2007). Lack of a role of membrane-protein interactions in flow-dependent activation of ENaC. *American Journal of Physiology: Renal Physiology* **293,** F316-324.

Carattino MD, Sheng S & Kleyman TR. (2004). Epithelial Na+ channels are activated by laminar shear stress. *Journal of Biological Chemistry* **279,** 4120-4126.

Chalfant ML, Denton JS, Berdiev BK, Ismailov, II, Benos DJ & Stanton BA. (1999). Intracellular H+ regulates the alpha-subunit of ENaC, the epithelial Na+ channel. *American Journal of Physiology: Cell Physiology* **276,** C477-486.

Chen W, Valamanesh F, Mirshahi T, Soria J, Tang R, Agarwal M & Mirshahi M. (2004). Aldosterone signaling modifies capillary formation by human bone marrow endothelial cells. *Vascular Pharmacology* **40,** 269-277.

Chlopicki S, Lomnicka M, Fedorowicz A, Grochal E, Kramkowski K, Mogielnicki A, Buczko W & Motterlini R. (2012). Inhibition of platelet aggregation by carbon monoxide-releasing molecules (CO-RMs): comparison with NO donors.

Naunyn-Schmiedeberg's archives of pharmacology **385,** 641-650.

Debonneville C, Flores SY, Kamynina E, Plant PJ, Tauxe C, Thomas MA, Münster C, Chraïbi A, Pratt JH & Horisberger JD. (2001). Phosphorylation of Nedd4-2 by Sgk1 regulates epithelial Na+ channel cell surface expression. *The EMBO Journal* **20,** 7052-7059.

Enuka Y, Hanukoglu I, Edelheit O, Vaknine H & Hanukoglu A. (2012). Epithelial sodium channels (ENaC) are uniformly distributed on motile cilia in the oviduct and the respiratory airways. *Histochemistry and Cell Biology* **137,** 339-353.

Evans RG & Bie P. (2015). Role of the kidney in the pathogenesis of hypertension: time for a neo-Guytonian paradigm or a paradigm shift? *American Journal of Physiology-Regulatory, Integrative and Comparative Physiology* **310,** R217-R229.

Ewing JF, Raju VS & Maines MD. (1994). Induction of heart heme oxygenase-1 (HSP32) by hyperthermia: possible role in stress-mediated elevation of cyclic 3':5'-guanosine monophosphate. *Journal of Pharmacology and Experimental Therapeutics* **271,** 408-414.

Firsov D, Schild L, Gautschi I, Mérillat A-M, Schneeberger E & Rossier BC. (1996). Cell surface expression of the epithelial Na channel and a mutant causing Liddle syndrome: a quantitative approach. *Proceedings of the National Academy of Sciences of the United States of America* **93,** 15370-15375.

Foresti R, Bani-Hani MG & Motterlini R. (2008). Use of carbon monoxide as a therapeutic agent: promises and challenges. *Intensive care medicine* **34,** 649-658.

Fronius M, Bogdan R, Althaus M, Morty RE & Clauss WG. (2010). Epithelial Na+

channels derived from human lung are activated by shear force. *Respiratory physiology & neurobiology* **170,** 113-119.

Fuchs W, Larsen EH & Lindemann B. (1977). Current-voltage curve of sodium channels and concentration dependence of sodium permeability in frog skin. *Journal of Physiology* **267,** 137-166.

Garcia-Gallego S & Bernardes GJ. (2014). Carbon-monoxide-releasing molecules for the delivery of therapeutic CO in vivo. *Angewandte Chemie International Ed In English* **53,** 9712-9721.

Garty H & Palmer LG. (1997). Epithelial sodium channels: function, structure, and regulation. *Physiological Reviews* **77,** 359-396.

Giraldez T, Rojas P, Jou J, Flores C & Alvarez de la Rosa D. (2012). The epithelial sodium channel delta-subunit: new notes for an old song. *American Journal of Physiology: Renal Physiology* **303,** F328-338.

Gorman D, Drewry A, Huang YL & Sames C. (2003). The clinical toxicology of carbon monoxide. *Toxicology* **187,** 25-38.

Haerteis S, Krueger B, Korbmacher C & Rauh R. (2009). The delta-subunit of the epithelial sodium channel (ENaC) enhances channel activity and alters proteolytic ENaC activation. *Journal of Biological Chemistry* **284,** 29024-29040.

Hager H, Kwon T-H, Vinnikova AK, Masilamani S, Brooks HL, Frøkiaer J, Knepper MA & Nielsen S. (2001). Immunocytochemical and immunoelectron microscopic localization of α-, β-, and γ-ENaC in rat kidney. *American Journal of Physiology-Renal Physiology* **280,** F1093-F1106.

Hamill OP & Martinac B. (2001). Molecular basis of mechanotransduction in living cells. *Physiological Reviews* **81,** 685-740.

Hanukoglu I & Hanukoglu A. (2016). Epithelial sodium channel (ENaC) family: Phylogeny, structure–function, tissue distribution, and associated inherited diseases. *Gene* **579,** 95-132.

Harvey KF, Dinudom A, Komwatana P, Jolliffe CN, Day ML, Parasivam G, Cook DI & Kumar S. (1999). All three WW domains of murine Nedd4 are involved in the regulation of epithelial sodium channels by intracellular Na+. *Journal of Biological Chemistry* **274,** 12525-12530.

Horowitz A, Menice CB, Laporte R & Morgan KG. (1996). Mechanisms of smooth muscle contraction. *Physiological Reviews* **76,** 967-1003.

Kamynina E, Debonneville C, Bens M, Vandewalle A & Staub O. (2001). A novel mouse Nedd4 protein suppresses the activity of the epithelial Na+ channel. *The FASEB Journal* **15,** 204-214.

Karpushev AV, Ilatovskaya DV & Staruschenko A. (2010). The actin cytoskeleton and small G protein RhoA are not involved in flow-dependent activation of ENaC. *BMC Research Notes* **3,** 210.

Kashlan OB & Kleyman TR. (2011). ENaC structure and function in the wake of a resolved structure of a family member. *American Journal of Physiology: Renal Physiology* **301,** F684-696.

Kim HH & Choi S. (2018). Therapeutic Aspects of Carbon Monoxide in Cardiovascular Disease. *International Journal of Molecular Sciences* **19**.

Kleyman TR, Carattino MD & Hughey RP. (2009). ENaC at the cutting edge: regulation of epithelial sodium channels by proteases. *Journal of Biological Chemistry* **284,** 20447-20451.

Knoepp F, Bettmer J & Fronius M. (2017). Gadolinium released by the linear gadolinium-based contrast-agent Gd-DTPA decreases the activity of human epithelial Na+ channels (ENaCs). *Biochimica et Biophysica Acta (BBA) - Biomembranes* **1859,** 1040-1048.

Lipowsky HH. (1995). Shear Stress in the Circulation. In *Flow-Dependent Regulation of Vascular Function*, ed. Bevan JA, Kaley G & Rubanyi GM, pp. 28-45. Springer New York, New York, NY.

Maines MD. (1997). The heme oxygenase system: a regulator of second messenger gases. *Annual Review of Pharmacology and Toxicology* **37,** 517-554.

Malik B, Yue Q, Yue G, Chen X, Price S, Mitch W & Eaton D. (2005). Role of Nedd4-2 and polyubiquitination in epithelial sodium channel degradation in untransfected renal A6 cells expressing endogenous ENaC subunits. *American Journal of Physiology: Renal Physiology* **289,** F107-F116.

Morita T, Mitsialis SA, Koike H, Liu Y & Kourembanas S. (1997). Carbon monoxide controls the proliferation of hypoxic vascular smooth muscle cells. *Journal of Biological Chemistry* **272,** 32804-32809.

NHBLI (2018). High Blood Pressure | National Heart, Lung, and Blood Institute (NHLBI). Nhlbinihgov. Available at: https://www.nhlbi.nih.gov/health-topics/high-blood-pressure [Accessed October 10, 2019].

Noreng S, Bharadwaj A, Posert R, Yoshioka C & Baconguis I. (2018). Structure of the human epithelial sodium channel by cryo-electron microscopy. *Elife* **7,** e39340.

Palmer LG. (1984). Voltage-dependent block by amiloride and other monovalent cations of apical Na channels in the toad urinary bladder. *Journal of Membrane Biology* **80,** 153-165.

Palmer LG & Andersen OS. (2008). The two-membrane model of epithelial transport: Koefoed-Johnsen and Ussing (1958). *Journal of General Physiology* **132,** 607-612.

Perez FR, Venegas F, Gonzalez M, Andres S, Vallejos C, Riquelme G, Sierralta J & Michea L. (2009). Endothelial epithelial sodium channel inhibition activates endothelial nitric oxide synthase via phosphoinositide 3-kinase/Akt in small-diameter mesenteric arteries. *Hypertension* **53,** 1000-1007.

Piantadosi CA. (2002). Biological chemistry of carbon monoxide. *Antioxid Redox Signal* **4,** 259-270.

Pratt JH. (2005). Central role for ENaC in development of hypertension. *Journal of the American Society of Nephrology* **16,** 3154-3159.

Rossier BC. (2014). Epithelial sodium channel (ENaC) and the control of blood pressure. *Current Opinion in Pharmacology* **15,** 33-46.

Rossier BC, Staub O & Hummler E. (2013). Genetic dissection of sodium and potassium transport along the aldosterone-sensitive distal nephron: importance in the control of blood pressure and hypertension. *FEBS Letters* **587,** 1929-1941.

Satlin LM, Sheng S, Woda CB & Kleyman TR. (2001). Epithelial Na+ channels are

regulated by flow. *American Journal of Physiology-Renal Physiology* **280,** F1010-F1018.

Schild L. (1996). The ENaC channel as the primary determinant of two human diseases: Liddle syndrome and pseudohypoaldosteronism. *Nephrologie* **17,** 395-400.

Schild L, Canessa CM, Shimkets RA, Gautschi I, Lifton RP & Rossier BC. (1995). A mutation in the epithelial sodium channel causing Liddle disease increases channel activity in the Xenopus laevis oocyte expression system. *Proceedings of the National Academy of Sciences of the United States of America* **92,** 5699-5703.

Schild L, Lu Y, Gautschi I, Schneeberger E, Lifton RP & Rossier BC. (1996). Identification of a PY motif in the epithelial Na channel subunits as a target sequence for mutations causing channel activation found in Liddle syndrome. *EMBO Journal* **15,** 2381-2387.

Sessa WC. (2004). eNOS at a glance. *Journal of Cell Science* **117,** 2427-2429.

Sharma K, Haque M, Guidry R, Ueta Y & Teruyama R. (2017). Effect of dietary salt intake on epithelial Na(+) channels (ENaC) in vasopressin magnocellular neurosecretory neurons in the rat supraoptic nucleus. *The Journal of Physiology* **595,** 5857-5874.

Sheng S, Bruns JB & Kleyman TR. (2004). Extracellular histidine residues crucial for Na+ self-inhibition of epithelial Na+ channels. *Journal of Biological Chemistry* **279,** 9743-9749.

Shi S, Ghosh DD, Okumura S, Carattino MD, Kashlan OB, Sheng S & Kleyman TR. (2011). Base of the thumb domain modulates epithelial sodium channel gating. *Journal*

of Biological Chemistry **286,** 14753-14761.

Shobair M, Dagliyan O, Kota P, Dang YL, He H, Stutts MJ & Dokholyan NV. (2016). Gain-of-function mutation W493R in the epithelial sodium channel allosterically reconfigures intersubunit coupling. *Journal of Biological Chemistry* **291,** 3682-3692.

Snyder PM, Price MP, McDonald FJ, Adams CM, Volk KA, Zeiher BG, Stokes JB & Welsh MJ. (1995). Mechanism by which Liddle's syndrome mutations increase activity of a human epithelial Na+ channel. *Cell* **83,** 969-978.

Song R, Mahidhara RS, Liu F, Ning W, Otterbein LE & Choi AM. (2002). Carbon monoxide inhibits human airway smooth muscle cell proliferation via mitogen-activated protein kinase pathway. *American Journal of Respiratory Cell and Molecular Biology* **27,** 603-610.

Staub O, Dho S, Henry P, Correa J, Ishikawa T, McGlade J & Rotin D. (1996). WW domains of Nedd4 bind to the proline-rich PY motifs in the epithelial Na+ channel deleted in Liddle's syndrome. *EMBO Journal* **15,** 2371-2380.

van den Berg BM, Nieuwdorp M, Stroes ES & Vink H. (2006). Glycocalyx and endothelial (dys) function: from mice to men. *Pharmacological Reports* **58 Suppl,** 75-80.

Verma A, Hirsch DJ, Glatt CE, Ronnett GV & Snyder SH. (1993). Carbon monoxide: a putative neural messenger. *Science* **259,** 381-384.

Waldmann R, Champigny G, Bassilana F, Voilley N & Lazdunski M. (1995). Molecular cloning and functional expression of a novel amiloride-sensitive Na+ channel. *Journal of Biological Chemistry* **270,** 27411-27414.

Wang S, Publicover S & Gu Y. (2009). An oxygen-sensitive mechanism in regulation of epithelial sodium channel. *Proceedings of the National Academy of Sciences of the United States of America* **106,** 2957-2962.

Wilkinson WJ & Kemp PJ. (2011). Carbon monoxide: an emerging regulator of ion channels. *The Journal of physiology* **589,** 3055-3062.

Yamamura H, Ugawa S, Ueda T, Nagao M & Shimada S. (2004). Protons activate the δ-subunit of the epithelial Na+ channel in humans. *Journal of Biological Chemistry* **279,** 12529-12534.

Ydegaard R, Andersen H, Oxlund CS, Jacobsen IA, Hansen PBL, Jurgensen JF, Peluso AA, Vanhoutte PM, Staehr M, Svenningsen P & Jensen BL. (2019). The acute blood pressure-lowering effect of amiloride is independent of endothelial ENaC and eNOS in humans and mice. *Acta Physiologica (Oxford, England)* **225,** e13189.

Zakhary R, Gaine SP, Dinerman JL, Ruat M, Flavahan NA & Snyder SH. (1996). Heme oxygenase 2: endothelial and neuronal localization and role in endothelium-dependent relaxation. *Proceedings of the National Academy of Sciences of the United States of America* **93,** 795-798.